JOURNAL OF GEOPHYSICAL RESEARCH, VOL. 103, NO. B8, PAGES 18,277–18,294, AUGUST 10, 1998

Thermal and compositional evolution of the shallow magma chambers of Vesuvius: Evidence from pyroxene phenocrysts and melt inclusions

Raffaello Cioni, Paola Marianelli, and Roberto Santacroce

Dipartimento di Scienze della Terra, Università degli Studi di Pisa, Pisa, Italy

Abstract. A large number of clinopyroxene (cpx) phenocrysts and hosted melt inclusions (MI) in pyroclasts from several Vesuvius eruptions were analyzed. Assuming that their temperature of homogenization (T_{hom}) reflects that of crystallization of the host mineral and that after homogenization and quenching, composition of the MI represents the melt from which the host crystallized, each cpx-MI pair records equilibrium conditions at T_{hom}. These data were used to discuss the magma evolution within shallow magma chamber. They formed by means of the periodic arrival of mafic batches, recorded by the MI in diopside (Fs_{4-7}) crystallized at 1150°-1200°C. Under open conduit conditions the chambers are small, and each magma pulse induces thermal and compositional variations recorded by oscillatory zoned pyroxenes (Fs_{4-15}). Their MI and T_{hom} summarize the evolution of the chamber resulting from cycles of magma injection, crystal settling, and magma extraction. The deposits of the explosive eruptions which reopen the conduit reflect variable mixing during magma withdrawal from zoned reservoirs, whose layering was deciphered through MI and T_{hom} in salite (Fs_{15-30}). We suggest that the Vesuvius magma chambers evolve from prolate toward subequant, changing their layering with increasing volume and age: (1) initial stage, high aspect ratio chamber, homogeneous mafic melt (T°C~1100) crystal enriched downward; (2) young stage, medium aspect ratio, continuous gradation from mildly evolved (T°C~1050) to felsic melt (T°C~850-900); and (3) mature stage, low aspect ratio, twofold chamber with stepwise gradient separating lower, convective, mildly evolved portion (T°C~1050) from upper, stratified, felsic portion (T°C~800-950).

1. Introduction

The highly variable activity recorded by Vesuvius reflects the occurrence of irregularly spaced periods of open and obstructed conduit conditions [*Santacroce*, 1983; *Civetta and Santacroce*, 1992; *Santacroce et al.*, 1994]. In both cases, there is evidence for the presence of shallow reservoirs periodically supplied by mafic magma batches [*Santacroce et al.*, 1993; *Cioni et al.*, 1995].

During open conduit periods (e.g., A.D. 1631-1944) the eruptive style ranges from quietly effusive to violent Strombolian and to strongly explosive, phreatomagmatic. The erupted magma volumes are in a range between <0.01 and 0.1×10^9 m^3, while the rock composition ranges from K-tephritic to K-tephriphonolitic. The largest events show complex, polyphased dynamics, accompanying the emission of magma whose variable bulk composition reflects a large variation in phenocryst content (e.g., 1906 and 1944 eruptions [*Santacroce et al.*, 1993; *Belkin et al.*, 1993; *Villemant et al.*, 1993]).

Eruptions marking reopening of the conduit after quiescent intervals of variable length are explosive, polyphased, and commonly characterized by a main, Plinian-type magmatic phase and initial and final phreatomagmatic phases. The erupted magmas have widely variable compositions (K-latite to K-trachyte; K-phonotephrite to K-alkaliphonolite) and volumes (0.2 to $>3\times10^9$ m^3).

Clinopyroxene is a common phenocryst phase of Vesuvius magmas [*Santacroce*, 1987], frequently hosting melt inclusions (MI). Assuming that (1) the temperature of homogenization (T_{hom}) of these inclusions is the (minimal) temperature of crystallization of the host mineral, and (2) after homogenization and quenching the composition of the included glass is representative of the melt from which the host mineral crystallized, each host-inclusion pair records equilibrium conditions at T_{hom}. They were used to decipher the main processes driving magma evolution during periods of open or obstructed conduit conditions.

Pyroxenes from pyroclasts, rather than from lavas, were studied because they represent a quenched record of the erupted magma. The MI are, in fact, glassy to cryptocrystalline with poor or absent crystallization of the host. In the studied crystals the homogenization process is reversible, showing that posttrapping transformations have been completely recovered and the system can be considered closed. Pyroxenes from lavas contain MI with trapped/daughter crystals [*Vaggelli et al.*, 1993] which are absent in the MI from Vesuvius pyroclasts. They give a T_{hom} [*Vaggelli et al.*, 1992; *Belkin et al.*, 1996] generally higher than those in pyroclasts. Several factors can cause such behavior. The relatively slow cooling of lava flows could induce nonreversible changes in the MI, thus promoting volatile diffusion and important crystallization. On the other hand, microfracturing of the host, possibly induced by pressure variations due to crystallization and vola-

Paper number 98JB01124.
0148-0227/98/98JB-01124$09.00

tile exsolution of the liquid in the MI, would favor an advective loss of volatiles.

2. Analytical Methods

More than 300 successful homogenization experiments were carried out on doubly polished wafers. Only glassy or cryptocrystalline MI, with a clear shrinkage bubble and no evidences of heterogeneous trapping [*Roedder*, 1984], were chosen. For the high-temperature experimental study of MI a modified Leitz 1350 heating stage and an optical heating stage, designed in the Vernadsky Institute of Geochemistry, Moscow (described by *Sobolev et al.* [1980], were used. The temperature was measured with a Pt-$Pt_{90}Rh_{10}$ thermocouple. The accuracy of measurement was around ±10°C (Leitz) and ±5°C (Vernadsky), controlled by the melting point of gold and silver. Experiments were performed in a He atmosphere. The rate of heating was varied as a function of the rate of transformation in the inclusions and ranged from 2 to 40°C/min to the point of complete homogenization of MI, i.e., disappearance of bubbles. At attainment of melt homogenization the samples were quenched (in air with Leitz and in He with the Vernadsky apparatus, for which the effective time of quenching was <1 s). After quenching, the inclusions were glassy, at times containing (experiments with Leitz) very small (1-2 μm) shrinkage bubbles on the wall of the inclusion. Some strongly zoned megacrysts were broken into several chips containing zones of differing composition, and thermometric measurements were carried out separately on inclusions in the different zones. Each fragment was quenched after attainment of homogenization of MI. Each crystal was then mounted in epoxy and gradually ground to the point of exposure of the inclusion. After final polishing, the glass inclusions were analyzed.

Quantitative analyses of the MI and of their host minerals were obtained by an Energy Dispersive System on a Scanning Electron Microscope (SEM-EDS) at Dipartimento di Scienze della Terra, University of Pisa (Philips 515 SEM with EDAX9900, Philips XL30 with EDAX DX4), at 20 kV accelerating energy, 200-500 nm beam diameter, 100 s live time (a raster area of about 10x10 μm was analyzed on glass). Where possible, three to five analyses were performed on each inclusion to check for its homogeneity. CFA47 trachytic, ALV981R23 basaltic, and KE12 pantelleritic glasses were used as reference standards (Table 1).

3. Studied Samples

Studied samples consist of phenocrysts (1-2 mm sized) from crushed coarse juvenile fragments from the deposits of five Plinian and sub-Plinian eruptions: A.D. 472 "Pollena," sub-Plinian [*Rosi and Santacroce*, 1983; *Marianelli*, 1995], A.D. 79 "Pompeii," Plinian [*Lirer et al.*, 1973, 1993; *Sheridan et al.*, 1981; *Sigurdsson et al.*, 1982, 1985, 1987; *Arnò et al.*, 1987; *Carey and Sigurdsson*, 1987; *Barberi et al.*, 1989; *Civetta et al.*, 1991; *Cioni et al.*, 1990, 1992, 1995], 3400 years B.P. "Avellino," Plinian [*Lirer et al.*, 1973; *Arnò et al.*, 1987; *Barberi et al.*, 1989; *Civetta et al.*, 1991; *Rolandi et al.*, 1993], and two sub-Plinian events, AP1 and AP4 [*Andronico et al.*, 1995], whose deposits are interbedded between those of Avellino and Pompeii. Loose clinopyroxene megacrysts (>5 mm) were directly picked from the fall deposits of the 1906 eruption. The presence of groundmass rim, quite similar to that of the associated scoriaceous lapilli, coating these pyroxenes indicates their juvenile origin. Five main different types of pyroxene were distinguished (Figure 1).

3.1. The 1906 Eruption

The crystals were collected from the top of the lapilli layer related to the lava fountain that preceded the final phreatomagmatic phases [*Bertagnini et al.*, 1991]. According to *Santacroce et al.* [1993], these lapilli resulted from the emission of a crystal-enriched magma from a shallow depth that formed as a result of repeated intrusions of tephritic magma, mixing, fractionation and extrusion of tephri-phonolitic differentiates. The crystals studied (type 5 in Figure 1) are euhedral to subeuhedral, prismatic parallel to *c*, up to 6 mm long and less than 3 mm in cross section, dark green or black in hand specimen, occasionally cracked or broken. The pyroxene texture is complex: the color darkens outward, often showing sector or oscillatory zoning. As remarked by

Table 1. Standard Analyses

	Metrich and Clocchiatti [1989]		*Fine and Stolper* [1986]	This Paper* (n=12)	
	Average	s.d.		Average	s.d.
			ALV 981 R23		
SiO_2	49.79	± 0.19	50.01	49.56	± 0.14
TiO_2	1.28	± 0.05	1.26	1.30	± 0.07
Al_2O_3	16.67	± 0.08	17.02	16.57	± 0.13
FeO	8.46	± 0.09	8.75	8.44	± 0.22
MnO	0.14	± 0.06	0.15	0.22	± 0.03
MgO	8.73	± 0.11	8.57	8.82	± 0.16
CaO	11.87	± 0.11	11.12	11.84	± 0.25
Na_2O	2.90	± 0.04	3.07	3.00	± 0.18
K_2O	0.05	± 0.01	0.05	0.10	± 0.05
S	0.12	± 0.00	nd	0.14	± 0.04
Total	100.00		100.00	100.00	
			CFA 47		
SiO_2	61.94	± 0.33		61.39	± 0.27
TiO_2	0.42	± 0.05		0.48	± 0.09
Al_2O_3	18.62	± 0.16		18.61	± 0.11
FeO	2.66	± 0.15		2.76	± 0.12
MnO	0.18	± 0.04		0.24	± 0.13
MgO	0.42	± 0.02		0.58	± 0.08
CaO	1.85	± 0.06		1.83	± 0.08
Na_2O	5.40	± 0.12		5.43	± 0.08
K_2O	8.02	± 0.16		8.14	± 0.04
Cl	0.49	± 0.01		0.54	± 0.08
Total	100.00			100.00	
	Metrich and Rutherford [1992]			This Paper* (n=10)	
	Average	s.d.		Average	s.d.
			KE 12		
SiO_2	70.83	± 0.22		70.80	± 0.23
TiO_2	0.28	± 0.02		0.31	± 0.06
Al_2O_3	7.82	± 0.03		7.92	± 0.16
FeO	8.67	± 0.20		8.41	± 0.06
MnO	0.29	± 0.03		0.38	± 0.07
MgO	nd			0.10	± 0.04
CaO	0.35	± 0 01		0.36	± 0.07
Na_2O	7.23	± 0.25		7.10	± 0.19
K_2O	4.19	± 0.15		4.29	± 0.07
Cl	0.33	± 0.00		0.32	± 0.08
Total	100.00			100.00	

Analyses of glass fragment normalized to 100.
* Philips XL30 with EDAX DX4, SEM-EDS analyses, DST, Università degli Studi di Pisa.
In parentheses number of quoted analyses; nd, not determined

				1 	2 	3 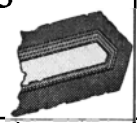	4 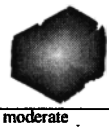	5 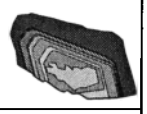
eruption	rock type	composition	CaO wt%	unzoned diopside (fs 4-7)	diopside-rimmed salite	large zoning diopside-salite (Fe.salite) (fs4-20 or more)	moderate direct zoning salite -fe.salite (fs15-30)	recurrent zoning diopside-salite
1906 Violent Strombolian	scoriaceous lapilli	tephriphonolite to phonolitictephrite	7-14	VERY RARE (microphenocrysts)		RARE	RARE	COMMON (megacrysts) (fs4-15)
A.D. 472 "POLLENA" Subpliman	pumiceous to scoriaceous lapilli	tephriticphonolite	5-8	RARE		RARE	PRESENT	
		tephrite	8-11	COMMON	VERY RARE	PRESENT	PRESENT	VERY RARE
A.D. 79 "POMPEII" Pliman	white pumice	phonolite	2-4	RARE		RARE	PRESENT	
	grey pumice	tephriticphonolite	5-8	PRESENT		RARE	PRESENT	
AP 4 sub-Pliman	pumiceous lapilli	tephriticphonolite	6-7		VERY RARE		COMMON	PRESENT (fs8-17)
AP 1 sub-Pliman	pumiceous lapilli	tephriticphonolite	5-8	RARE	VERY RARE	RARE	COMMON	
3,400 yr BP "AVELLINO" Pliman	white pumice	phonolite	1-5-3	RARE			RARE	
	grey pumice	tephriticphonolite	4-7	PRESENT	VERY RARE	RARE	PRESENT	

Figure 1. Pyroxene occurrence.

Thompson [1972], the crystals invariably show sharp breaks to a paler color and gradations to a darker color, with irregular growth surfaces. The largest pyroxenes often contain a colorless, skeletal, unzoned core surrounded by a distinctly Fe-rich zone (green), which consists of numerous small oscillatory zones.

The crystals are frequently characterized by films of vesiculated brown glass filling cracks and cleavage surfaces (Figure 2). As the preservation of an inclusion depends on its size [*Tait*, 1992], we interpret this feature as the result of abrupt decompression of the largest MI during eruption. "Unexploded" primary MI were distinguished both in green and colorless zones. In colorless cores the MI (50-60 μm) are completely cryptocrystalline ("devitrified"); smaller rounded glass inclusions (glass + shrinkage bubble ± minute crystal nuclei) occur along the growth surfaces of the host crystals, mainly in the greenish zones.

3.2. A.D. 472 "Pollena"

Pyroxene phenocrysts were separated from composite pumice or scoria samples from the fallout (VS88.38 and VS88.40 from the base, VS88.48 from the top) as well as from interbedded pyroclastic flow (SM55, SM63) and the final surge deposits (VS88.51). These samples fully cover the compositional variation of the eruption sequence (Figure 3 and Table 2). Millimeter-sized euhedral pyroxenes, optically unzoned and colorless (type 1 in Figure 1), are common in tephritic (VS88.51) and phonotephritic samples (SM63, SM55, VS88.48) and absent in most evolved phonolitic samples (VS88.38, VS88.40) (Table 2). These pyroxenes contain randomly distributed, completely crystallized MI (20-60 μm). Larger inclusions (>100 μm), also cryptocrystalline, occur sporadically, often associated with cracks, which penetrate the host mineral. Euhedral, pleochroic type 4 green pyroxenes prevalently occur in phonotephritic and phonolitic samples, while strongly zoned type 3, at times showing recurrent zoning (type 5), is common only in phonotephritic samples. Two-phase (glass+shrinkage bubble) inclusions (15-40 μm) are present in the green portions of these pyroxenes, showing moderate or no devitrification. At a visual inspection, bubble size correlates with inclusion size.

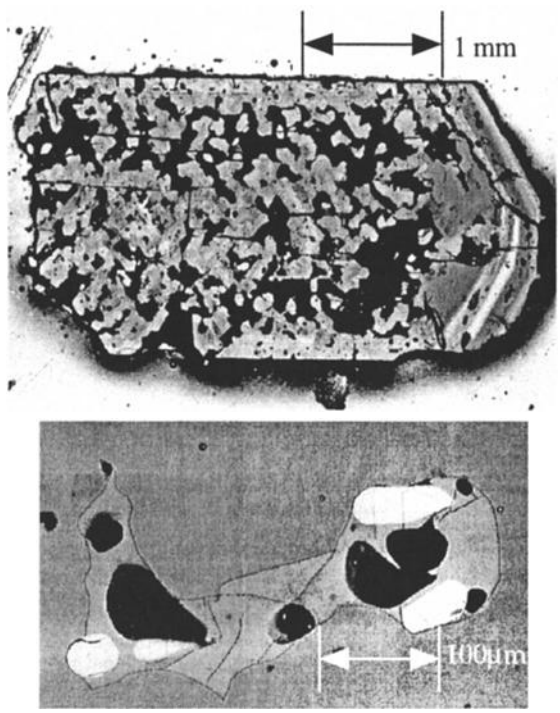

Figure 2. (top) Strongly zoned pyroxene megacryst from 1906 eruption. Drops of vesiculated brown glass spread along cracks and cleavage surfaces are interpreted as due to abrupt decompression of the biggest melt inclusions during eruption. (bottom) Backscattered SEM image showing vesicles (black) and crystals (white) in the brown glass.

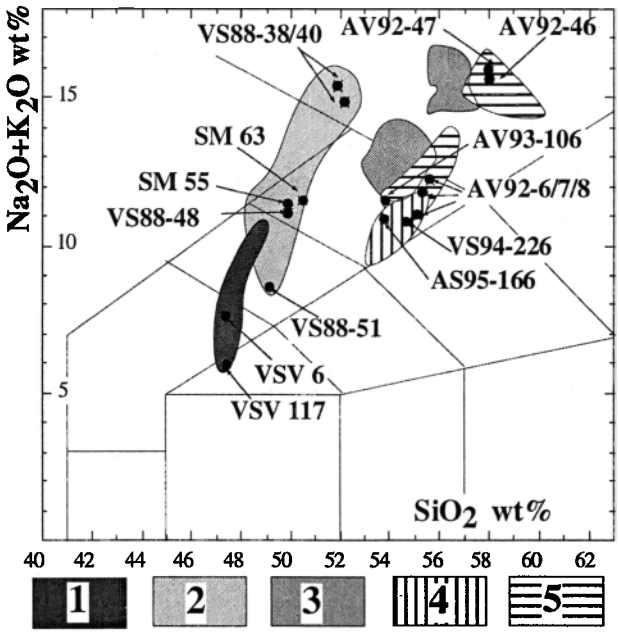

Figure 3. Total Alkali versus Silica diagram [*Le Bas et al.*, 1986] of products from selected Vesuvius eruptions (data from *Cioni et al.* [1995], *Santacroce et al.* [1993], *Marianelli* [1995], and unpublished [1996]): 1, 1906: 2, "Pollena"; 3, "Pompeii"; 4, AP-1 & AP-4, 5, "Avellino." Samples hosting studied pyroxenes are indicated. The 1906 samples refer to lapilli layers hosting loose megacrysts.

3.3. A.D. 79 "Pompeii"

Data on pyroxenes and their MI are from *Marianelli et al.* [1995] and *Cioni et al.* [1995]. They mostly refer to type 1 crystals separated from samples covering the entire depositional sequence (phonolite to tephriphonolite). Relatively rare, green pyroxene microphenocrysts are present in all pumice samples.

3.4. AP1 and AP4 Eruptions

Minerals were from tephriphonolitic samples (AS95-166 and VS94-226) of the central portion of the compositional field of the two eruptions (Figure 3 and Table 2). Type 4 greenish, normally zoned pyroxenes are very common in all samples. In AP1, type 3 pyroxene is present, characterized by a colorless core sharply passing to a moderately zoned green outer portion. The color transition is often crowned by small (20 μm), subspherical, two-phase MI (brown glass and shrinkage bubble). Type 1 pyroxene is rarely present in AP1 only, whereas in the AP4 pumice, recurrently zoned euhedral type 5 phenocrysts are present, which rarely show a colorless core. MI are distributed in all the different zones.

3.5. The 3400 Years B.P. "Avellino"

The studied crystals are from grey tephriphonolitic upper (AV93-106, AV92-6, AV92-7, AV92-8) and white phonolitic lower (AV92-46, AV92-47) fall deposits (Figure 3 and Table 2). As in the A.D. 79 pumice, types 1 and 4 pyroxenes are common, irrespective of the composition of the host pumice. Colorless crystals rarely exhibit a thin greenish rim. Primary MI are relatively common in both types. As in similar crystals from other eruptions, the MI in type 1 pyroxene (20-60 μm) are cryptocrystalline, while in green pyroxene they are subspherical and glassy, with one or more bubbles.

4. Results

4.1. The 1906 Eruption

4.1.1. Mineral chemistry. The well-developed oscillatory zoning of the pyroxene was quantitatively defined through tightly spaced spot analyses along selected profiles (Figure 4). Within one 1.6-mm traverse between the diopside core and the salite rim (phenocryst from an unspecified Vesuvius lava), *Thompson* [1972] recognized 44 major oscillatory zones. In the analyzed samples, up to at least 17 different zones were recognized. Sector zoning is frequently developed in the mantles and is superimposed on the oscillatory zoning.

As is well known from a long history of mineralogical studies [*Zambonini*, 1910; *Lacroix*, 1917; *Washington and Merwin*, 1921; *Thompson*, 1972; *Rahman*, 1975], a notable feature of Vesuvius pyroxenes is their wide Al_2O_3 range. In studied samples it extends from 2 to 10 wt %, in some cases within individual crystals, correlating well with iron and titanium (Figure 5). Table 3 shows that these pyroxenes contain substantial amounts of Fe^{3+} (Fe^{2+} can be practically absent). According to *Thompson* [1972] the main coupled substitutions explaining the observed chemical variations are $Fe^{3+}Al$ and 2 Fe^{3+} for MgSi and Ti2(Al, Fe^{3+}) for Mg2Si. The substitution 2Al for MgSi seems infrequent, and Al probably does not occur in octahedral structural sites of the Mg-richest zones.

4.1.2. Optical thermometry. T_{hom} measured on partially or totally crystallized MI along the growth surfaces of three different pyroxene crystals, ranges from T_{hom} 1060 to 1200°C (Figure 6). Within single crystals, the MI show variable T_{hom}, increasing with a decreasing Fe content of the host zone (Figure 4).

Recent measurements on MI in clinopyroxene phenocrysts of lapilli from the 1906 eruption [*Santacroce et al..*, 1993] gave a higher T_{hom} (1250°-1216°C). This discrepancy has to be related to the longer duration of these experiments (10 hours) when compared with the three hour-long experiments carried out for our work. The difference in T_{hom} (50°-70°C) could result from volatile diffusion, as suggested by *Sobolev et al.* [1993].

4.1.3. MI and host rock compositions. After homogenization and quenching, the glass inclusions exhibit K-tephritic to K-tephriphonolitic compositions, with a MgO content from 2.3 to 6.6, increasing with T_{hom}. Representative MI analyses are reported in Table 4 and compared with whole rock compositions in Figure 7. The glass compositions mostly cover the variation range of erupted products.

4.2. Plinian and Sub-Plinian Eruptions

4.2.1. Mineral chemistry. In pumice from all Vesuvius Plinian and sub-Plinian eruptions pyroxene phenocrysts have a compositional range from diopside to fassaitic ferrosalite. Although the compositional range is the same, the frequency of occurrence of the pyroxene compositions differ in the four eruptions studied (Figure 8).

The distribution of the main cations of these pyroxenes as a function of calculated Si occupancy of tetraedric sites shows moderate differences in the Ti content only. The Pollena py-

Table 2. Chemical Analyses of Host Rocks

	Eruption							
	3400 years B.P.						AP1	AP4
	AV92-47	AV92-46	AV92-6	AV92-7	AV92-8	AV93-106	VS94-226	AS95-166
SiO_2	58.03	58.02	55.61	55.39	54.69	53.78	55.07	53.76
TiO_2	0.11	0.13	0.44	0.47	0.54	0.54	0.59	0.75
Al_2O_3	22.07	22.08	19.31	18.82	18.43	18.55	18.42	18.59
Fe_2O_3 tot	1.78	1.86	4.22	4.45	5.03	4.99	5.05	6.51
MnO	0.12	0.12	0.13	0.13	0.13	0.13	0.13	0.14
MgO	0.25	0.35	2.47	2.72	3.29	3.5	2.82	2.44
CaO	1.69	1.72	5.42	5.82	6.74	6.77	6.58	6.57
Na_2O	8.84	8.59	5.39	5.2	4.44	4.54	4.33	3.78
K_2O	7.09	7.12	6.78	6.64	6.38	6.89	6.69	7.07
P_2O_5	0.01	0.02	0.24	0.25	0.33	0.31	0.31	0.38
Zr, ppm	816	795	419	375	334	348	270	256
Ba	145	193	905	1013	1096	1109	1136	1588
Sr	169	187	524	561	609	605	739	883
Rb	519	517	355	340	310	321	324	335
Cr	4	4	52	54	77	53	56	31
Co	2	3	14	13	17	16	16	20
Ni	3	3	23	27	33	27	25	13
Nb	144	140	74	65	58	60	45	47
Cl	4199	4131	3563	3184	3334	2943	nd	nd
S	140	174	382	369	365	395	nd	nd
	Eruption							
	A.D. 472						1906	
	VS88-38b	VS88-40b	SM63	VS88-48	SM55	VS88-51	VSV6	VSV117
SiO_2	51.84	52.15	50.48	49.89	49.82	49.15	47.5	47.5
TiO_2	0.51	0.53	0.78	0.87	0.83	0.75	0.99	0.97
Al_2O_3	20.48	20.25	18.07	17.4	17.81	15.38	14.7	13
Fe_2O_3 tot	5.09	5.19	6.71	7.35	7.13	6.53	9	8.6
MnO	0.15	0.15	0.14	0.16	0.15	0.13	0.16	0.15
MgO	0.88	1.16	3.27	3.28	3.4	7.23	6.7	8.9
CaO	5.51	5.62	8.58	9.35	9.2	11.84	12.8	14.2
Na_2O	6.25	5.74	3.57	3.38	3.47	2.65	2	1.6
K_2O	9.16	9.03	7.96	7.85	7.75	5.81	5.5	4.3
P_2O_5	0.13	0.18	0.42	0.48	0.46	0.55	0.78	0.79
Zr, ppm	214	199	199	197	203	165	184	152
Ba	2157	2305	2377	2509	2401	1608	1420	1193
Sr	1671	1629	1360	1350	1345	874	820	638
Rb	246	258	285	287	284	236	217	169
Cr	8	10	51	45	55	226	152	206
Co	12	12	20	23	22	24	nd	nd
Ni	5	6	23	24	24	68	55	82
Nb	101	92	50	42	47	17	25	19
Cl	6272	6082	4108	4394	4172	3614	nd	nd
S	520	554	458	414	433	373	nd	nd

XRF analyses recalculated water-free to 100; all Fe as Fe_2O_3; nd, not determined.

roxenes are slightly Ti-richer than Avellino and AP pyroxenes (Figure 9), while the Pompeii pyroxene extends throughout the compositional field. Average representative analyses are reported in Table 5.

The type 1 crystals (Figure 1) are diopsidic ($En_{51-41}Wo_{43-51}Fs_{3-9}$) independently of either the eruption or the composition of the host pumice. The single crystals are approximately homogeneous in composition (Figure 10).

The type 3 pyroxene is generally characterized by a diopsidic core bound by a thick directly zoned mantle with a quite continuous compositional transition between contiguous zones. In the Avellino and Pompeii products, no relation is apparent between the extent of zonation and the composition of the host rock. In the Avellino products the full recorded compositional variation occurs in pyroxene from both grey tephriphonolitic and white phonolitic pumice, forming a continuous series.

The type 4 pyroxene is represented by normally zoned salitic phenocrysts and microphenocrysts whose compositional range is variable in the different eruptions, as well as in different samples from the same eruption and (Avellino and Pompeii grey pumice) in different crystals from the same sample. In the Pollena sequence the degree of evolution of the host rock directly relates to the Fe content of the outer pyroxene zones. In the Avellino and Pompeii sequences the Fe-richest rims (Fs=25-30%) occur in pyroxenes from both white phonolitic and grey tephriphonolitic pumice.

4.2.2. Optical thermometry. Optical thermometry measurements were performed on MI in pyroxene crystals from different samples of the five Plinian-type eruptions

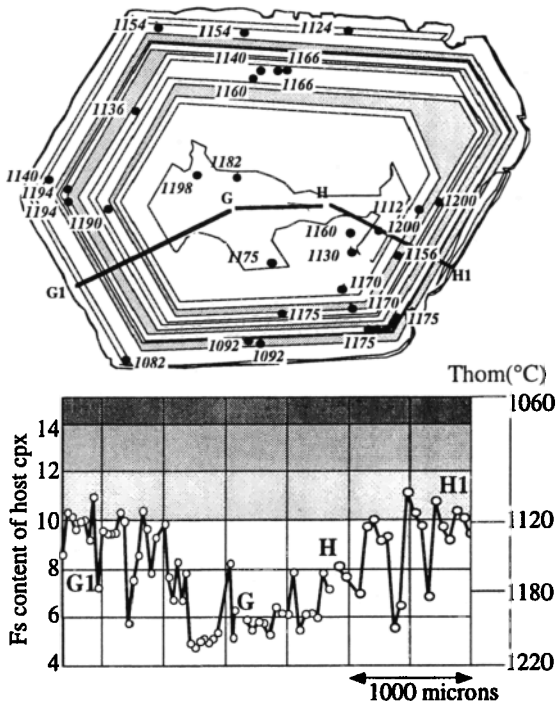

Figure 4. (top) Schematic drawing of a recurrently zoned 1906 megacryst. Dots show location of melt inclusions with measured T_{hom}. G1-G-H-H1 is the trace of the analyzed profile. (bottom) Fs variations along the indicated profile compared with T_{hom} of melt inclusions occurring in the zones cut by the profile.

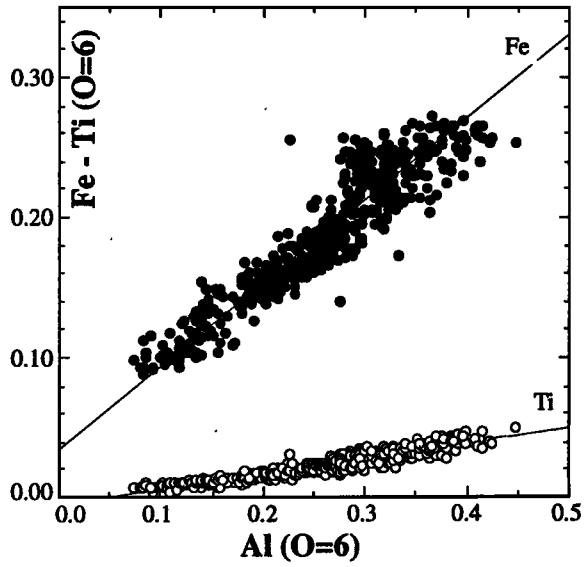

Figure 5. Al (O=6) versus Fe and Ti plot of pyroxene from 1906 eruption.

studied (Figure 8). Note that the Pompeii data only refer to unzoned diopside [*Marianelli et al.*, 1995; *Cioni et al.*, 1995]. Irrespective of the composition of the host rock, MI in type 1 pyroxene homogenized between 1100°C and 1180°C. MI from the types 3 and 4 pyroxenes have a wider T_{hom} range (800°-1100°C), inversely correlating the Fs content of the host mineral (Figure 11). For the same temperature the Pollena pyroxene seems Fs richer than the Avellino and AP pyroxene. This is probably due to the lower silica activity of the Pollena melts.

4.2.3. MI and host rock compositions. After homogenization and quenching, MI in pyroxene show greatly variable compositions (Figure 12 and Table 6). As already stressed by *Marianelli et al.* [1995], MI in diopside have high MgO (>6.0 wt %) and CaO (>12 wt %) contents, with K-basaltic compositions characterizing Avellino and AP products and K-tephritic compositions characterizing Pollena products. Both compositions were found in the Pompeiii inclusions. MI in types 2 and 3 pyroxene have greatly variable

Table 3. Average Compositions of Pyroxene Megacrysts From 1906 Eruption

n	12	32	30	60	63	75	52	46	72	51	11
SiO_2	51.93	51.45	50.98	49.95	49.03	48.30	47.63	47.02	46.78	46.01	44.76
TiO_2	0.27	0.32	0.40	0.53	0.68	0.78	0.88	1.01	1.14	1.29	1.40
Al_2O_3	2.20	2.86	3.39	4.46	5.28	6.02	6.52	7.18	7.39	8.12	8.87
FeO*	3.12	3.49	4.13	4.79	5.30	5.90	6.44	6.97	7.54	8.08	8.56
MnO	0.13	0.13	0.11	0.13	0.17	0.14	0.14	0.13	0.16	0.16	0.19
MgO	17.53	17.12	16.57	15.80	15.20	14.62	14.08	13.56	13.12	12.53	11.87
CaO	23.95	23.56	23.43	23.38	23.33	23.33	23.31	23.09	23.09	23.12	23.62
Na_2O	0.56	0.87	0.86	0.83	0.87	0.78	0.88	0.90	0.66	0.70	0.73
Cr_2O_3	0.31	0.19	0.14	0.14	0.14	0.14	0.12	0.14	0.12	0.00	0.00
Wo	47.17	47.03	47.13	47.63	47.98	48.33	48.63	48.71	48.89	49.33	50.45
En	48.04	47.54	46.39	44.77	43.51	42.14	40.88	39.81	38.65	37.21	35.28
Fs	4.80	5.43	6.48	7.61	8.51	9.53	10.49	11.48	12.47	13.45	14.26
Recalculated to Four Cations											
Si	1.88	1.86	1.85	1.82	1.79	1.77	1.74	1.73	1.73	1.70	1.66
Ti	0.01	0.01	0.01	0.01	0.02	0.02	0.02	0.03	0.03	0.04	0.04
Al	0.09	0.12	0.15	0.19	0.23	0.26	0.28	0.31	0.32	0.35	0.39
Fe	0.09	0.11	0.13	0.15	0.16	0.18	0.20	0.21	0.23	0.25	0.27
Mn	0.00	0.00	0.00	0.00	0.01	0.00	0.00	0.00	0.01	0.01	0.01
Mg	0.95	0.92	0.90	0.86	0.83	0.80	0.77	0.74	0.72	0.69	0.66
Ca	0.93	0.91	0.91	0.91	0.91	0.91	0.91	0.91	0.91	0.92	0.94
Na	0.04	0.06	0.06	0.06	0.06	0.06	0.06	0.06	0.05	0.05	0.05
Cr	0.01	0.01	0.00	0.00	0.00	0.00	0.00	0.00	0.00	0.00	0.00
Fe^{3+}	0.16	0.20	0.20	0.20	0.22	0.22	0.24	0.24	0.21	0.22	0.27
Fe^{2+}	-0.07	-0.09	-0.07	-0.06	-0.06	-0.04	-0.04	-0.03	0.02	0.03	-0.01

n, number of quoted analyses. FeO*, all Fe as FeO.

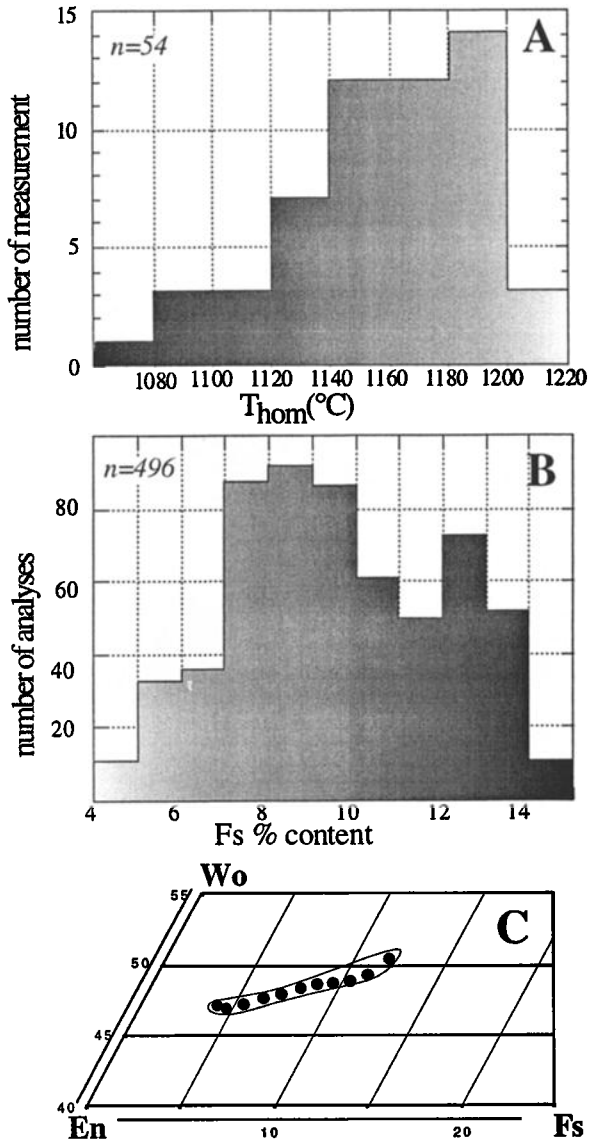

Figure 6. The 1906 clinopyroxene. All data refer to megacrysts and phenocrysts from fallout deposits of the final phases of the eruption. They should reflect the ejection of a pyroxene crystal mush forming since 1872 after repeated intrusions of tephritic magma, mixing, fractionation, and extrusion of tephritic-phonolitic differentiates [*Santacroce et al.*, 1993]. (a) Histogram of measured temperatures of homogenization (T_{hom}) of melt inclusions in pyroxene. (b) Histogram of 1906 pyroxene composition expressed as ferrosilite %. (c) Plot of pyroxene mean composition (Figure 1) within a portion of the En-Wo-Fs triangle.

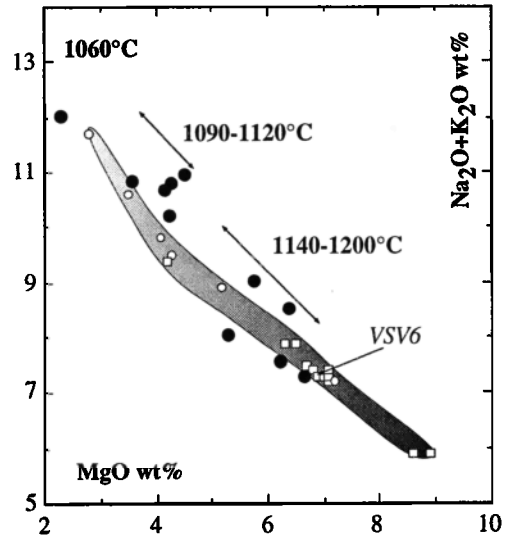

Figure 7. Composition of homogenized melt inclusions in 1906 pyroxene (solid dots) compared with whole rock analyses of 1906 lavas (circles) and pyroclasts (squares). Data from *Santacroce et al.* [1993]. The T_{hom} range is indicated as well as the analyzed sample (VSV6) from the lapilli layer hosting studied megacrysts. The compositional variation of 1906 lava and lapilli is mostly conditioned by their content in pyroxene phenocrysts, whose increasing content is qualitatively suggested by the darkening of the shaded field.

compositions (CaO=10-4 wt %) which logarithmically correlate with T_{hom} (Figure 12). Therefore the CaO (or MgO, Al_2O_3) content can be used to evaluate the temperature of natural purely glassy MI, relatively abundant in the Pollena products (Table 7). The plot of [Na_2O+K_2O] content of MI as a function of CaO results in two different variation trends: a "Pollena trend" which is strongly silica-undersaturated and a slightly undersaturated "Avellino AP trend". They are nearly continuous from basalt-tephrite to phonolite, expanding the fields depicted by whole rock compositions (Figure 12).

5. Discussion

In recent papers [*Santacroce et al.*, 1993, 1998; *Marianelli et al.*, 1995; *Cioni et al.*, 1995] we have discussed the feeding of Vesuvius shallow magma chambers within the carbonate "basement" (deeper than 2-3 km [*Bernasconi et al.*, 1981]) or in the upper volcanic and volcanoclastic pile. These chambers grow with the arrivals of mafic magma batches which thermally equilibrate and mix with the cooler, resident

Table 4. Chemical Composition of Homogenized MI in Pyroxenes From 1906 Eruption: Sample VSV6

	px4b	px4e	px4e	px1a	px4b	px4g	px1i	px1i	px4g	px3	px1g	px1g
Fs host	12.86	9.60	10.08	8.71	8.93	6.76	7.93	7.93	6.76	6.05	6.70	9.23
T_{hom}, °C	1060	1092	1112	1118	1120	1136	1144	1144	1154	1170	1199	nd
SiO_2	55.10	52.04	50.96	49.62	49.89	50.64	48.20	47.39	48.75	50.74	48.09	48.42
TiO_2	1.18	1.15	1.25	1.07	1.11	1.10	1.01	1.38	1.29	0.76	1.48	1.04
Al_2O_3	18.75	18.75	17.66	17.25	17.19	14.88	15.08	15.87	14.73	16.37	15.73	17.26
FeO	4.28	4.97	5.61	5.90	6.17	6.58	7.08	8.12	7.75	6.01	7.55	6.89
MnO	0.14	0.16	0.27	0.16	0.09	0.18	0.12	0.24	0.15	0.10	0.17	0.16
MgO	2.30	3.61	4.19	4.54	4.26	6.40	5.78	5.32	6.65	5.51	6.27	4.31
CaO	5.60	7.99	8.76	9.78	10.58	11.20	13.22	13.24	12.97	9.84	12.70	10.64
Na_2O	2.77	2.78	2.71	3.06	2.89	2.27	2.46	2.27	1.90	3.01	2.26	3.17
K_2O	9.26	8.08	7.98	7.91	7.31	6.26	6.55	5.76	5.39	7.13	5.34	7.64
Cl	0.63	0.48	0.62	0.70	0.52	0.49	0.49	0.41	0.42	0.52	0.41	0.47

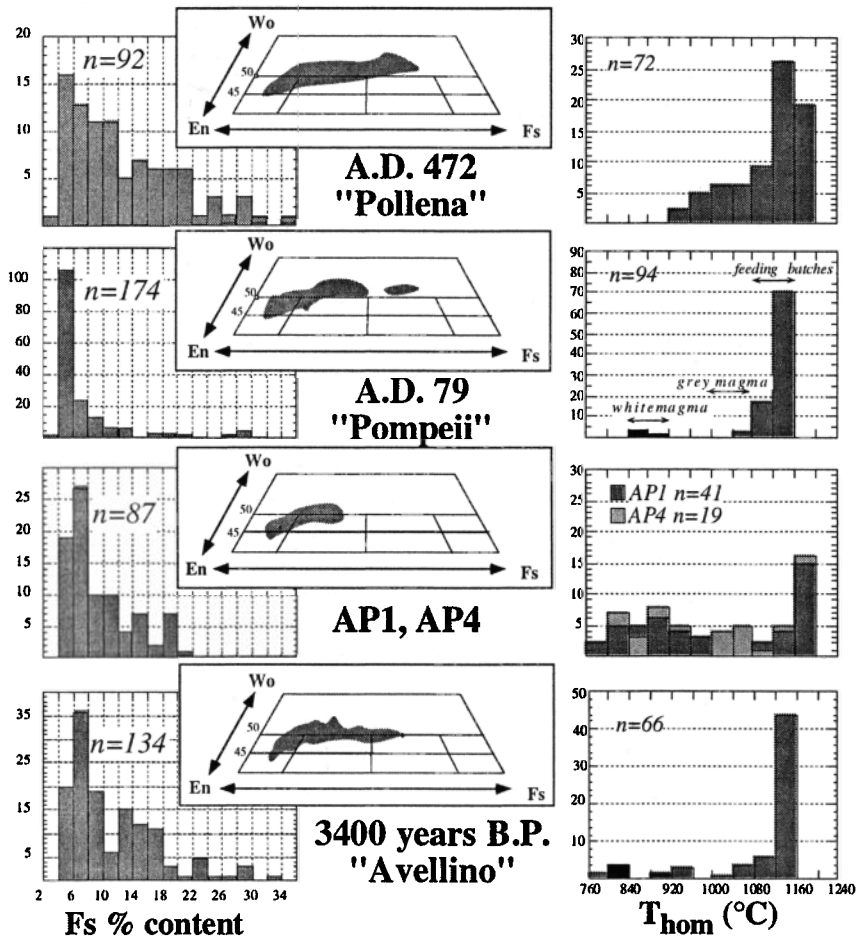

Figure 8. (left) Fs% of analyzed Plinian pyroxenes of Vesuvius (n is number of analyses). (middle) Fields of pyroxene composition within a portion of the En-Wo-Fs triangle. (right) T_{hom} frequency histogram measured on MI in pyroxene. Some data on MI in sanidine [*Barberi et al.*, 1981; our unpublished data, 1996] are also reported (solid); the Pompeiii chamber was formed by an overheated "grey" magma capped by a white phonolitic cap: the temperatures estimated for both bodies [*Cioni et al.*, 1995] are indicated.

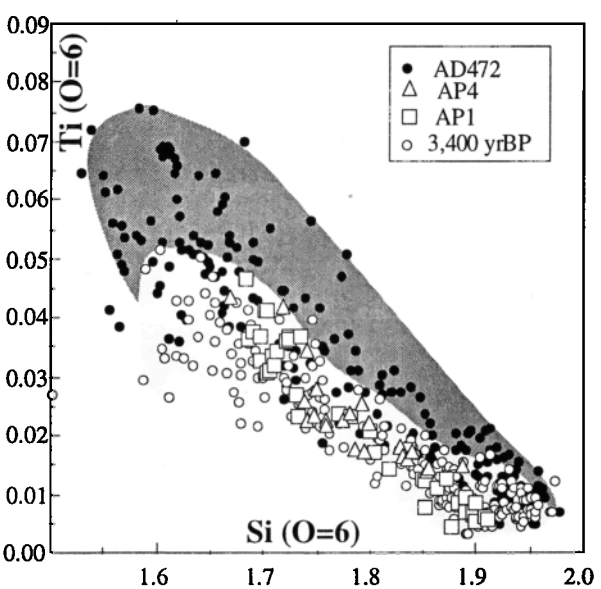

Figure 9. Si(O=6) versus Ti diagram of pyroxene from "Plinian" and "sub-Plinian" eruptions.

magma. An example of these batches was recognized in the 1906 eruption (tephritic "B feeding unit": T°C = 1150-1200; mass of 1-2 × 10^{10} kg; density of 2500-2800 kg/m^3; viscosity of 400-4000 P [*Santacroce et al.*, 1993]).

When the conduit is open, the reservoir is continuously tapped through persistent Strombolian activity. The periodic arrival of fresh magma in the full plumbing system results in eruptions whose dynamics can episodically induce the complete emptying of the reservoir ("Final Eruptions" [*Santacroce*, 1983; *Civetta and Santacroce*, 1992]). After short quiescent periods (reflecting the recharge of the system), Strombolian conditions are restored. The present 54 year long quiescent period departs from the 1631-1944 pattern (7 years maximum length of repose between cycles [*Carta et al.*, 1981]). The conclusion is that the 1944 eruption marks the transition to obstructed conduit conditions [*Santacroce et al.*, 1998; *Quareni and Mulargia*, 1993].

When the conduit is obstructed a magma chamber forms and grows until a explosive eruption is initiated. The variable magnitude of these eruptions reflects the variable degree of emptying (partial or total depending on eruption dynamics) of chambers of varying size and depth. Whatever the magnitude of the eruption, the deposits are all characterized by geo-

Table 5. Average Compositions of Pyroxene Phenocrysts From Plinian and sub-Plinian Eruptions

	Eruption												
	3400 years B.P.								AP1				
n	20	55	21	18	4	6	4	1	4	15	4	2	2
SiO_2	52.17	50.50	46.46	45.83	43.57	42.87	42.09	41.87	52.45	51.55	49.54	47.68	46.66
TiO_2	0.24	0.46	0.97	0.95	1.17	1.35	1.46	1.36	0.23	0.35	0.57	0.79	1.00
Al_2O_3	1.95	3.27	8.08	8.00	10.17	9.62	10.11	10.27	1.72	2.60	4.67	6.24	6.77
FeO*	3.49	4.86	7.66	9.63	11.83	13.64	16.31	18.04	3.63	4.54	5.66	8.10	9.41
MnO	0.11	0.50	0.13	0.26	0.18	0.27	0.48	0.80	0.16	0.16	0.18	0.13	0.28
MgO	17.63	16.01	12.69	11.91	9.73	8.76	6.63	5.70	17.55	17.07	15.45	12.57	11.47
CaO	23.64	24.18	23.91	23.30	23.36	23.49	22.34	21.96	23.49	23.22	23.43	23.92	23.64
Na_2O	0.39	ld	ld	ld	ld	ld	0.59	ld	0.43	0.39	0.40	0.54	0.54
Cr_2O_3	0.39	0.23	0.11	0.11	ld	ld	ld	ld	0.34	0.26	0.18	0.05	0.47
Wo	46.44	48.11	50.27	49.25	50.65	50.65	50.42	49.94	46.29	45.97	47.49	50.11	50.35
En	48.22	44.33	37.15	34.89	29.32	26.35	20.84	18.04	48.12	47.01	43.56	36.65	34.00
Fs	5.34	7.56	12.58	15.86	20.03	23.01	28.75	32.02	5.59	7.02	8.95	13.24	15.65
Recalculated to Four Cations													
Si	1.89	1.85	1.72	1.71	1.64	1.63	1.62	1.63	1.90	1.88	1.81	1.77	1.74
Ti	0.01	0.01	0.03	0.03	0.03	0.04	0.04	0.04	0.01	0.01	0.02	0.02	0.03
Al	0.08	0.14	0.35	0.35	0.45	0.43	0.46	0.47	0.07	0.11	0.20	0.27	0.30
Fe	0.11	0.15	0.24	0.30	0.37	0.43	0.52	0.59	0.11	0.14	0.17	0.25	0.29
Mn	0.00	0.02	0.00	0.01	0.01	0.01	0.02	0.03	0.00	0.00	0.00	0.00	0.01
Mg	0.95	0.87	0.70	0.66	0.55	0.50	0.38	0.33	0.95	0.93	0.84	0.69	0.64
Ca	0.92	0.95	0.95	0.93	0.94	0.96	0.92	0.92	0.91	0.91	0.92	0.95	0.95
Na	0.03						0.04		0.03	0.03	0.03	0.04	0.04
Cr	0.01	0.01	0.00	0.00					0.01	0.00	0.00	0.00	0.01
Fe^{3+}	0.14	0.13	0.14	0.17	0.19	0.23	0.27	0.19	0.13	0.14	0.16	0.19	0.20
Fe^{2+}	-0.03	0.02	0.09	0.13	0.18	0.21	0.26	0.40	-0.02	0.00	0.01	0.06	0.10

	Eruption												
	AP1		AP4							A.D.79			
n	2	14	14	1	5	4	5	5	2	103	39	12	4
SiO_2	45.55	45.35	45.35	51.79	50.14	49.10	47.83	46.83	45.81	52.63	50.53	46.70	44.24
TiO_2	1.48	1.24	1.24	0.54	0.63	0.71	0.81	1.02	1.19	0.43	0.70	1.13	1.51
Al_2O_3	8.02	7.31	7.31	2.57	4.41	5.07	6.06	6.81	8.11	1.63	3.51	7.83	9.15
FeO*	10.27	11.52	11.52	4.47	5.44	6.88	8.08	9.48	10.05	3.30	4.86	7.00	9.68
MnO	0.25	0.38	0.38	ld	0.14	0.18	0.18	0.22	0.21	0.15	0.17	0.22	0.18
MgO	10.57	10.00	10.00	16.11	15.14	14.17	12.93	11.92	11.15	17.24	15.57	12.92	10.66
CaO	23.39	23.46	23.46	23.87	23.53	23.39	23.47	23.11	22.68	23.96	24.11	23.53	24.06
Na_2O	0.41	0.64	0.64	0.55	0.45	0.46	0.55	0.58	0.71	0.34	0.38	0.50	0.44
Cr_2O_3	0.07	0.14	0.14	0.09	0.12	0.07	0.12	ld	0.15	0.33	0.17	0.17	0.07
Wo	50.72	50.61	50.61	47.95	48.18	48.26	49.13	49.08	49.29	47.43	48.64	50.10	51.78
En	31.91	30.00	30.00	45.04	43.13	40.66	37.67	35.20	33.67	47.48	43.70	38.27	31.94
Fs	17.37	19.39	19.39	7.00	8.69	11.07	13.21	15.72	17.04	5.09	7.66	11.63	16.27
Recalculated to Four Cations													
Si	1.71	1.71	1.71	1.89	1.84	1.81	1.77	1.74	1.71	1.91	1.85	1.72	1.65
Ti	0.04	0.04	0.04	0.01	0.02	0.02	0.02	0.03	0.03	0.01	0.02	0.03	0.04
Al	0.35	0.32	0.32	0.11	0.19	0.22	0.26	0.30	0.36	0.07	0.15	0.34	0.40
Fe	0.32	0.36	0.36	0.14	0.17	0.21	0.25	0.30	0.31	0.10	0.15	0.22	0.30
Mn	0.01	0.01	0.01	0.00	0.00	0.00	0.00	0.01	0.01	0.00	0.01	0.01	0.01
Mg	0.59	0.56	0.56	0.88	0.83	0.78	0.71	0.66	0.62	0.93	0.85	0.71	0.59
Ca	0.94	0.95	0.95	0.93	0.92	0.92	0.93	0.92	0.91	0.93	0.95	0.93	0.96
Na	0.03	0.05	0.05	0.04	0.03	0.03	0.04	0.04	0.05	0.02	0.03	0.04	0.03
Cr	0.00	0.00	0.00	0.00	0.00	0.00	0.00	0.00	0.00	0.01	0.00	0.00	0.00
Fe^{3+}	0.17	0.23	0.23	0.12	0.14	0.15	0.19	0.20	0.21	0.10	0.13	0.18	0.23
Fe^{2+}	0.15	0.13	0.13	0.02	0.03	0.06	0.06	0.10	0.11	0.00	0.01	0.04	0.07

Table 5. (continued)

	Eruption											
	A.D.79				A.D.472							
n	4	1	8	3	17	24	16	13	12	4	4	2
SiO_2	43.32	41.99	40.76	39.57	53.09	50.96	48.47	44.81	44.22	40.68	41.52	41.77
TiO_2	1.62	1.44	1.62	1.66	0.39	0.69	1.09	1.67	1.85	2.88	2.41	1.99
Al_2O_3	9.75	10.86	11.01	11.93	1.29	2.54	4.12	8.07	6.96	10.08	8.94	7.98
FeO*	11.75	13.64	16.06	18.01	3.17	5.23	7.34	9.40	12.04	13.90	15.62	18.75
MnO	0.31	0.12	0.57	0.56	0.19	0.21	0.24	0.34	0.42	0.43	0.54	0.76
MgO	9.26	8.42	6.24	4.72	17.21	15.07	13.46	10.78	9.57	7.58	6.70	5.17
CaO	23.22	22.70	22.34	22.64	23.77	24.58	24.65	24.23	24.12	23.58	23.57	22.98
Na_2O	0.74	0.82	1.22	0.91	0.47	0.48	0.44	0.52	0.62	0.69	0.57	0.53
Cr_2O_3	0.03	ld	0.20	ld	0.42	0.23	0.19	0.19	0.19	0.18	0.14	0.08
Wo	51.28	50.37	51.30	52.33	47.35	49.52	50.19	52.04	51.50	52.43	52.29	51.28
En	28.46	26.00	19.92	15.18	47.72	42.25	38.14	32.21	28.43	23.44	20.68	16.06
Fs	20.26	23.63	28.78	32.49	4.93	8.23	11.67	15.75	20.07	24.13	27.04	32.66
	Recalculated to Four Cations											
Si	1.63	1.59	1.56	1.53	1.93	1.87	1.80	1.68	1.67	1.55	1.60	1.63
Ti	0.05	0.04	0.05	0.05	0.01	0.02	0.03	0.05	0.05	0.08	0.07	0.06
Al	0.43	0.48	0.50	0.54	0.06	0.11	0.18	0.36	0.31	0.45	0.41	0.37
Fe	0.37	0.43	0.51	0.58	0.10	0.16	0.23	0.29	0.38	0.44	0.50	0.61
Mn	0.01	0.00	0.02	0.02	0.01	0.01	0.01	0.01	0.01	0.01	0.02	0.03
Mg	0.52	0.47	0.36	0.27	0.93	0.83	0.74	0.60	0.54	0.43	0.38	0.30
Ca	0.94	0.92	0.92	0.94	0.93	0.97	0.98	0.97	0.98	0.96	0.97	0.96
Na	0.05	0.06	0.09	0.07	0.03	0.03	0.03	0.04	0.05	0.05	0.04	0.04
Cr	0.00	0.00	0.01	0.00	0.01	0.01	0.01	0.01	0.01	0.01	0.00	0.00
Fe^{3+}	0.27	0.32	0.38	0.37	0.09	0.14	0.19	0.23	0.28	0.32	0.29	0.29
Fe^{2+}	0.10	0.11	0.14	0.21	0.01	0.02	0.03	0.06	0.10	0.12	0.21	0.32

n, number of quoted analyses; FeO*, all Fe as FeO; ld, below detection limit.

chemical and isotopic gradients, indicating that the chambers were always compositionally zoned. As a first approximation, the higher the degree of magma evolution, the older the age of the chamber (i.e., the length of the repose preceding the eruption) and the greater the magnitude of the eruption.

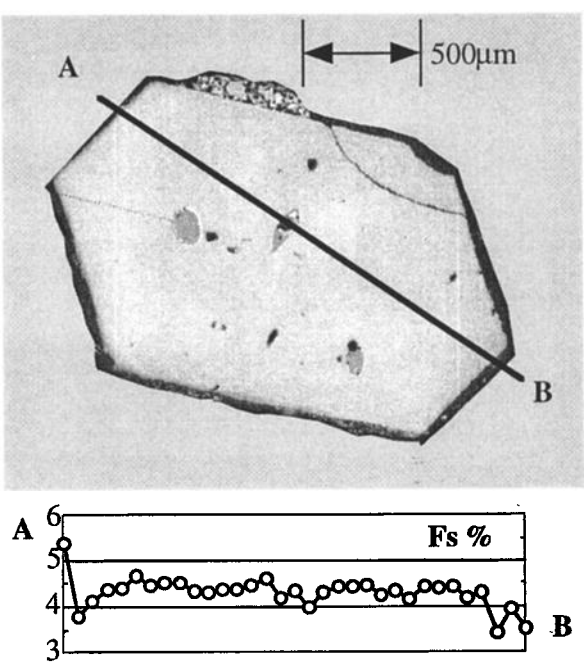

Figure 10. Backscattered SEM image of a typical unzoned "Plinian" diopside. The analyzed profile shows the almost constant composition of the mineral.

5.1. The Different Pyroxenes and Their Signifcance

The different types of pyroxene phenocrysts and their MI are crucial in reconstructing the thermal and compositional evolution of melt within the chambers. Their distribution within the different eruption phases also provides information about the dynamics of magma withdrawal during eruptions.

5.1.1. Types 1-2: Mafic magma supplying the chambers. The unzoned diopside type 1 was found in all the studied eruptions, mainly concentrated in the final phases of Plinian and sub-Plinian events. The mineral chemistry and composition and the T_{hom} of the MI reveal that they crystallized from mafic, K-tephritic to K-basaltic magmas, at a temperature of 1100°-1200°C. Significant differences in pyroxene composition or in T_{hom} of a "basaltic" or "tephritic" MI are not apparent. These pyroxenes could have formed as a result of depressurization during the ascent of the mafic batches supplying the chambers (higher T terms, Figures 6 and 8), and/or by crystallization while reaching thermal equilibrium before mixing with magma resident in the lower portions of the chamber [*Marianelli et al.*, 1995; *Cioni et al.*, 1995]. The latter formed within a temperature range depending on the equilibrium temperature (approximate temperature of resident magma, due to the mass ratio) and then rapidly segregated to supply the crystal mush plastering the inner-lower walls of the chamber. From there they were uprooted during eruption. This process was chiefly active during those eruptive phases involving high vorticity or roof collapse in the chamber (e.g., "Pompeii" eruption [*Cioni et al.*, 1995]).

A similar origin can be invoked for type 2 pyroxene (salite with thin diopside rim). We suggest that salitic cores record

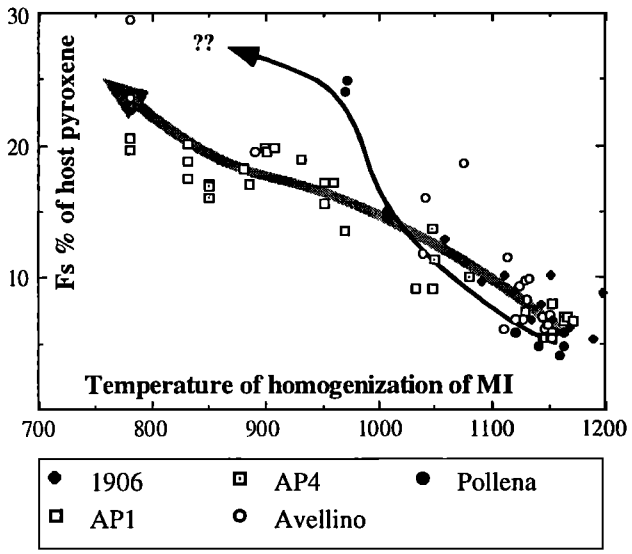

Figure 11. The temperatures of homogenization of MI in pyroxene as a function of the calculated Fs% of the host mineral depict a well-defined "Avellino AP" trend and suggest a diverging trend for Pollena products. This is due to the higher silica undersaturation of Pollena magmas (for a given temperature, Fe-richer pyroxene forms in melts with lower silica activity).

suspended crystals in the resident magma incorporated in the hot mafic plume, which then follow the segregation and withdrawal history of type 1 pyroxenes. Furthermore, the absence of this type of crystal in the Pompeii grey pumice is consistent with the hypothesized overheated state of magma occupying the lower portion of the Pompeii chamber [*Cioni et al.*, 1995].

5.1.2. Types 3-4: Magma in Plinian and sub-Plinian chambers. The type 3 pyroxenes (zoned crystals from diopside to salite) represent zoned suspended crystals in the resident magma, growing on diopsidic cores from the mafic batches, after avoiding rapid segregation. The type 4 pyroxenes (zoned salite) must also be interpreted as suspended crystals. They form and grow within the evolving resident magma. Their generally undisturbed direct zoning indicates that they crystallized without suffering abrupt thermal/compositional perturbations related to the discrete arrivals of new mafic batches, due to the large size of the chamber. These crystals with their MI help to reconstruct the cooling histories of the Vesuvius Plinian and sub-Plinian chambers and illustrate their thermal conditions just before the eruption. MI and T_{hom} data were used to define, within a Total Alkali versus Silica diagram (Figure 13a), the composition-temperature field of Vesuvius magmas. We can compare theoretical equilibrium fractionation trends (calculated with the "MELTS" program of *Ghiorso and Sack* [1995]) with the actual trends defined by MI as well as by whole rock analyses (Figure 13b). The theoretical trends appear "shorter" than the observed ones, equilibrium fractionation being apparently unable to reach phonolitic compositions. In our view, the possibility of producing at Vesuvius such highly evolved compositions solely results from the repeated refilling of the chambers [*O'Hara*, 1977], inducing the "incompatible behavior" of alkalies (chiefly K) over a compositional range wider than in closed system equilibrium fractionation. As a consequence of the periodic refilling, in fact, the chamber melts evolve with a smoother thermal slope than in closed system conditions (Figure 14), and the temperature of extensive K-feldspar crystallization (~900°C) is reached at very high alkali concentrations.

5.1.3. Type 5: Thermal state of magma chambers during open conduit conditions. The magma chambers that characterize open conduit conditions are small (10^7-10^8 m^3 [*Santacroce*, 1983; *Santacroce et al.*, 1993]). The recurrent zoning of type 5 pyroxene, mostly from the 1906 eruption, can be interpreted in terms of the relevant thermal and compositional variations induced in such chambers by each newly arrived magma batch.

According to *Santacroce et al.* [1993], the 1906 magma chamber had developed since 1872 with a complex pattern of fresh magma refilling and partial tapping. A semiquantitative approach to the problem was attempted by making a rough calculation of its possible thermal evolution. Using input data forced to fit volume, phenocryst, and trace element contents of magma erupted during the 1872-1906 period [*Santac-*

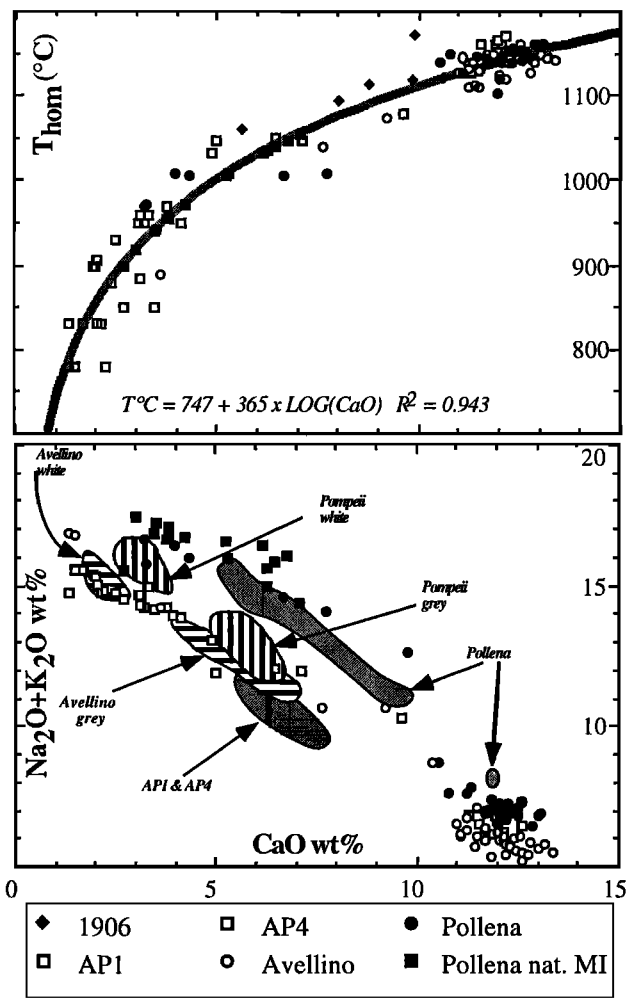

Figure 12. (top) The CaO content of MI logarithmically correlates the temperature of homogenization (curve and function are reported). The calculated temperatures of Pollena natural, unheated MI (Table 7) are shown. (bottom) CaO versus (Na_2O+K_2O) variation diagram of whole rocks (fields) and MI in pyroxene. Whole rock data are from *Cioni et al.* [1995], *Marianelli* [1995], and unpublished [1996].

Table 6. Chemical Composition of Homogenized MI in Pyroxenes From Plinian and sub-Plinian Eruptions

Fs host	T_{hom}, °C	N	n	SiO_2	TiO_2	Al_2O_3	FeO	MnO	MgO	CaO	Na_2O	K_2O	Cl
							3400 years B.P. Avellino Eruption						
26.6 ± 4.4	780	2	6	56.99 ± 0.45	0.18 ± 0.12	22.74 ± 0.05	1.20 ± 0.07	0.11 ± 0.04	0.19 ± 0.12	1.39 ± 0.11	6.94 ± 0.15	9.79 ± 0.10	0.47 ± 0.04
19.5	890	1	2	57.94	0.35	20.11	2.65	0.13	0.67	3.59	5.02	9.15	0.40
15.5 ± 3.5	1051	3	6	52.51 ± 0.42	0.84 ± 0.15	19.17 ± 1.57	5.08 ± 0.96	0.20 ± 0.08	2.66 ± 0.59	9.03 ± 1.39	2.89 ± 0.29	7.10 ± 0.91	0.51 ± 0.10
8.6 ± 1.9	1122	9	25	51.79 ± 0.62	1.00 ± 0.08	15.67 ± 1.02	6.76 ± 0.89	0.11 ± 0.08	6.21 ± 0.97	11.60 ± 0.56	1.75 ± 0.24	4.76 ± 0.56	0.35 ± 0.08
6.1 ± 0.9*	1147	22	78	51.53 ± 0.63	0.95 ± 0.09	14.58 ± 0.95	7.11 ± 0.62	0.07 ± 0.08	7.28 ± 0.55	12.26 ± 0.57	1.61 ± 0.14	4.24 ± 0.33	0.36 ± 0.03
							AP1 Eruption						
20.1 ± 0.6	780	2	3	57.87 ± 0.07	0.38 ± 0.05	21.21 ± 0.52	2.54 ± 0.60	0.16 ± 0.01	0.29 ± 0.03	1.85 ± 0.55	4.94 ± 0.27	10.18 ± 0.23	0.58 ± 0.04
19.1 ± 1.2	830	4	9	58.45 ± 0.74	0.35 ± 0.06	21.19 ± 0.26	2.24 ± 0.45	0.11 ± 0.02	0.39 ± 0.13	1.78 ± 0.39	5.06 ± 0.30	9.87 ± 0.43	0.56 ± 0.08
19.3 ± 0.7	903	5	9	58.34 ± 0.61	0.31 ± 0.14	21.16 ± 0.52	2.06 ± 0.18	0.05 ± 0.05	0.34 ± 0.13	2.16 ± 0.25	5.13 ± 0.28	9.87 ± 0.33	0.57 ± 0.03
16.4 ± 1.6	957	6	9	57.01 ± 0.31	0.46 ± 0.09	20.49 ± 0.50	2.88 ± 0.23	0.09 ± 0.04	0.71 ± 0.18	3.40 ± 0.42	4.74 ± 0.09	9.61 ± 0.33	0.60 ± 0.04
7.4	1128	1	4	50.00	0.87	17.06	7.57	0.10	5.99	11.23	2.35	4.47	0.37
7.1 ± 0.5	1163	5	15	50.41 ± 0.57	0.91 ± 0.07	16.18 ± 0.42	6.52 ± 0.38	0.10 ± 0.08	7.18 ± 0.56	11.99 ± 0.40	2.33 ± 0.07	4.08 ± 0.32	0.30 ± 0.06
							AP4 Eruption						
17.0 ± 0.1	867	2	5	58.10 ± 0.95	0.38 ± 0.11	21.42 ± 0.06	1.79 ± 0.80	0.08 ± 0.02	0.40 ± 0.13	2.89 ± 0.30	4.62 ± 0.19	9.72 ± 0.33	0.59 ± 0.16
10.8 ± 2.2	1044	4	7	55.27 ± 1.36	0.49 ± 0.05	19.39 ± 0.59	3.89 ± 0.68	0.14 ± 0.06	2.24 ± 0.39	5.82 ± 1.10	3.94 ± 0.39	8.25 ± 0.63	0.57 ± 0.05
10.1	1079	1	2	52.28	0.49	17.33	5.22	0.00	4.35	9.55	3.90	6.39	0.51
							A.D. 79 Pompei Eruption						
6.1 ± 0.9†	1138	11	37	50.70 ± 0.86	1.22 ± 0.10	14.87 ± 0.51	7.19 ± 0.54	0.16 ± 0.05	6.71 ± 0.21	12.16 ± 0.79	1.95 ± 0.18	4.62 ± 0.21	0.43 ± 0.12
6.3 ± 0.5†	1149	4	19	50.28 ± 0.58	1.18 ± 0.02	14.10 ± 0.61	7.55 ± 0.47	0.15 ± 0.06	7.17 ± 0.11	12.68 ± 0.87	2.00 ± 0.24	4.44 ± 0.23	0.45 ± 0.06
6.6 ± 0.8†	1139	12	36	50.27 ± 0.60	1.12 ± 0.19	14.81 ± 0.95	6.90 ± 0.82	0.15 ± 0.05	6.51 ± 0.30	11.93 ± 0.55	2.08 ± 0.45	5.69 ± 0.47	0.53 ± 0.21
5.5 ± 0.5†	1145	14	39	50.65 ± 0.72	1.14 ± 0.11	13.69 ± 0.56	7.12 ± 0.48	0.16 ± 0.05	7.60 ± 0.25	12.33 ± 0.56	1.80 ± 0.15	5.05 ± 0.35	0.46 ± 0.17
							A.D. 472 Pollena Eruption						
24.4 ± 0.6	971	2	2	53.77 ± 0.69	0.34 ± 0.03	21.78 ± 0.15	3.05 ± 0.27	0.16 ± 0.06	0.83 ± 0.21	3.20 ± 0.05	6.03 ± 0.64	10.03 ± 1.26	0.82 ± 0.11
14.8 ± 0.2	1007	2	4	53.37 ± 0.35	0.47 ± 0.11	21.58 ± 0.21	2.66 ± 0.13	0.08 ± 0.12	0.91 ± 0.15	4.12 ± 0.25	3.94 ± 0.06	12.19 ± 0.26	0.68 ± 0.09
14.8 ± 0.3	1007	2	4	52.66 ± 0.12	0.56 ± 0.10	20.96 ± 0.19	2.92 ± 0.04	0.14 ± 0.01	0.69 ± 0.14	7.16 ± 0.76	3.70 ± 0.07	10.54 ± 0.43	0.67 ± 0.04
6.2 ± 0.6	1116	3	7	50.93 ± 1.01	1.19 ± 0.21	13.97 ± 1.21	7.86 ± 0.72	0.14 ± 0.12	7.30 ± 0.06	11.62 ± 0.53	1.73 ± 0.17	4.80 ± 0.65	0.45 ± 0.04
5.4 ± 0.8*	1150	23	93	51.00 ± 0.57	1.01 ± 0.10	14.33 ± 0.91	6.75 ± 0.45	0.13 ± 0.07	7.03 ± 1.01	11.90 ± 0.80	1.93 ± 0.33	5.46 ± 0.98	0.46 ± 0.10

T_{hom}, homogenization temperature of MI; N, number of quoted MI; n, number of quoted analyses.
*, Data also from *Marianelli et al.* [1995].
†, Data also from *Marianelli et al.* [1995] and *Cioni et al.* [1995].

Table 7. Chemical Composition of Natural MI in Pyroxenes and Glass Matrix From A.D. 472 Eruption

T_c, °C	SiO_2	TiO_2	Al_2O_3	FeO	MnO	MgO	CaO	Na_2O	K_2O	Cl
				Natural Glass Inclusions						
1055	50.24	0.25	20.26	6.25	0.25	0.88	6.90	8.45	5.56	0.98
1035	55.53	0.45	19.39	2.70	0.00	0.26	6.08	10.77	3.78	1.03
900	56.54	0.16	22.06	2.10	0.06	0.52	2.61	10.56	4.67	0.70
1036	50.03	0.72	21.40	4.88	0.00	0.54	6.11	7.16	8.10	1.05
1040	49.97	0.19	22.45	4.55	0.00	0.29	6.31	8.99	6.47	0.78
1009	52.02	0.24	21.36	4.41	0.00	0.33	5.18	8.31	7.34	0.81
1048	49.35	0.20	22.16	4.80	0.00	0.30	6.60	9.04	6.67	0.87
1032	49.96	0.58	22.49	4.48	0.00	0.31	6.05	9.38	6.76	0.00
1007	52.19	0.37	21.72	4.12	0.00	0.15	5.16	9.66	6.63	0.00
954	53.01	0.22	21.72	4.02	0.00	0.27	3.66	7.79	8.42	0.89
972	52.46	0.11	21.78	4.21	0.00	0.25	4.11	9.53	6.79	0.77
957	52.50	0.46	21.69	4.13	0.00	0.31	3.72	8.68	7.65	0.87
941	53.08	0.10	22.56	3.15	0.00	0.43	3.37	8.67	7.79	0.85
956	52.75	0.13	21.78	3.78	0.00	0.32	3.70	8.68	7.94	0.91
942	53.37	0.40	22.32	3.37	0.00	0.15	3.43	8.46	8.50	0.00
918	53.28	0.03	22.75	2.92	0.00	0.20	2.92	8.77	8.23	0.90

n	SiO_2 s.d.	TiO_2 s.d.	Al_2O_3 s.d.	FeO s.d.	MnO	MgO s.d.	CaO s.d.	Na_2O s.d.	K_2O s.d.	Cl s.d.
				Glass Matrix						
43	50.53 ± 0.97	0.40 ± 0.06	22.89 ± 0.54	4.53 ± 0.57	nd	0.74 ± 0.03	5.75 ± 0.80	9.01 ± 1.76	5.97 ± 2.05	1.13 ± 0.46
22	53.07 ± 1.57	0.33 ± 0.07	22.84 ± 1.08	3.95 ± 1.02	nd	0.37 ± 0.15	4.12 ± 1.11	10.96 ± 1.79	4.17 ± 1.23	1.04 ± 0.85
35	50.63 ± 2.10	3.40 ± 0.11	23.25 ± 1.53	3.81 ± 1.56	nd	0.67 ± 0.19	4.42 ± 1.70	11.89 ± 3.09	4.81 ± 2.84	1.52 ± 0.98
30	49.58 ± 0.89	0.49 ± 0.07	22.50 ± 0.40	4.62 ± 0.83	nd	1.10 ± 0.25	5.94 ± 1.10	8.36 ± 1.48	7.26 ± 2.52	0.97 ± 0.19
31	50.03 ± 0.89	0.50 ± 0.07	22.65 ± 0.50	4.87 ± 0.55	nd	1.04 ± 0.19	5.83 ± 0.81	9.15 ± 1.91	5.77 ± 1.94	1.15 ± 0.28
27	49.74 ± 1.16	0.56 ± 0.11	22.41 ± 0.74	5.18 ± 0.82	nd	1.45 ± 0.42	5.89 ± 1.07	9.39 ± 0.94	5.26 ± 1.22	1.09 ± 0.27
30	49.60 ± 1.43	0.77 ± 0.15	21.26 ± 0.79	7.02 ± 1.33	nd	1.40 ± 0.66	7.61 ± 1.75	6.86 ± 2.69	5.30 ± 3.22	0.97 ± 0.39
30	50.18 ± 0.65	0.63 ± 0.09	21.89 ± 0.28	6.17 ± 0.55	nd	1.41 ± 0.21	5.79 ± 0.81	9.06 ± 0.53	4.71 ± 0.47	1.16 ± 0.10
87	49.84 ± 1.08	0.65 ± 0.12	21.85 ± 0.60	6.12 ± 0.90	nd	1.42 ± 0.43	6.43 ± 1.21	8.44 ± 1.39	5.09 ± 1.64	1.08 ± 0.25

T_c, calculated temperature for MI compositions; n, number of quoted analyses; nd, not determined.

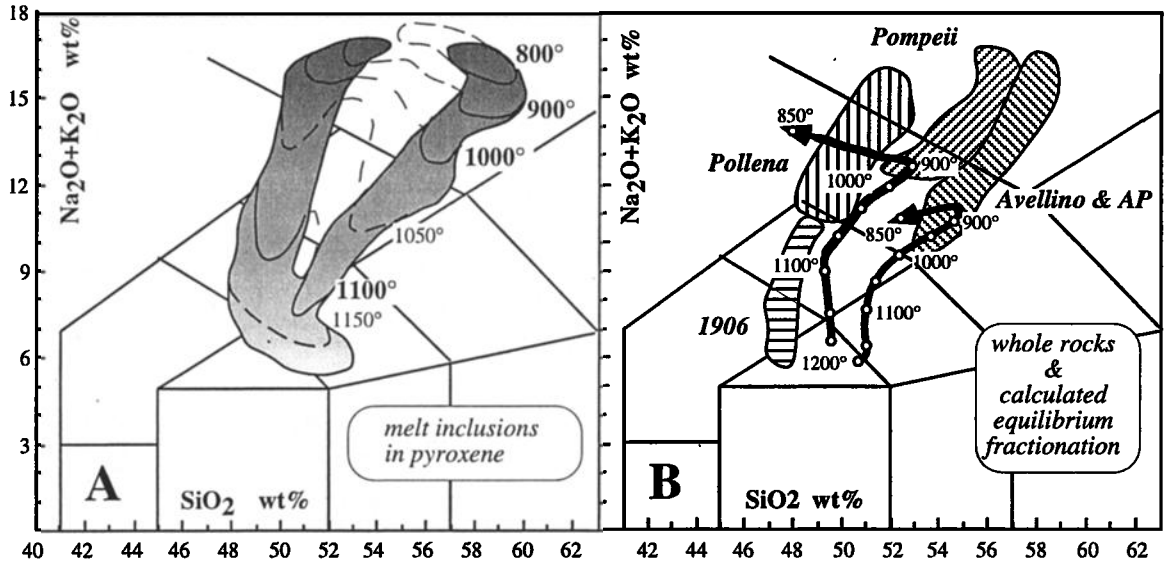

Figure 13. Total Alkali versus Silica diagrams [*Le Bas et al.*, 1986] comparing (a) MI and (b) whole rock compositions. The measured T_{hom} and calculated temperatures allow the definition of the temperature-composition field of Vesuvius magmas (Figure 13a). It seems inconsistent with closed-system equilibrium fractionation trends (arrowed lines in Figure 13b) calculated through the "MELTS" program [*Ghiorso and Sack*, 1995] at 1.5 kbar from initial melts with H_2O=2.0 - 2.2 wt % (compositions from *Marianelli et al.* [1995]).

roce et al., 1993], we have modeled a possible thermal path of the chamber (Figure 15), which illustrates the temperature oscillations recorded in the pyroxenes. The chamber is assumed to grow through a 35-year interval following a cyclic pattern of refilling, Rayleigh fractionation, and partial tapping. Each cycle begins with the arrival of a new mafic batch (5×10^6 m^3, T°C=1200 [*Santacroce et al.*, 1994]). This batch mixes with the resident magma and proceeds with the crystallization (2 vol %) and extraction of constant amounts of mixed magma (calculated by dividing the volume of magma erupted during the 1872-1906 cycle of Vesuvius, 40×10^6 m^3, by the number of cycles, 30). The model very simply calcu-

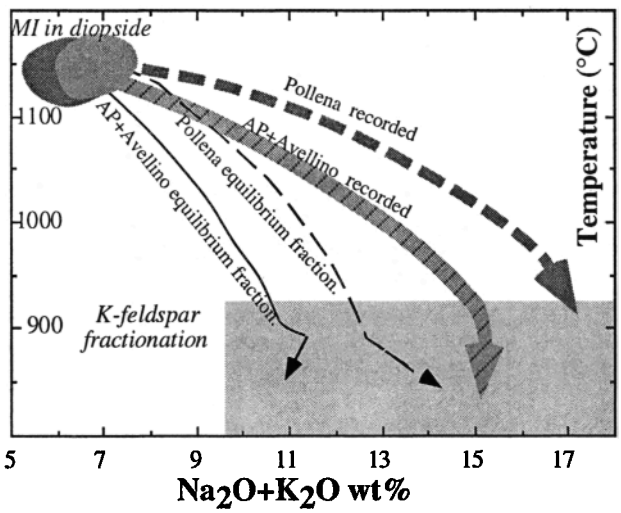

Figure 14. (Na_2O+K_2O) versus temperature plot showing that starting from the same initial liquid, Vesuvius (refilled) chambers reach the temperature of extensive K-feldspar fractionation when the alkali content is significantly higher than in conditions of closed system equilibrium fractionation.

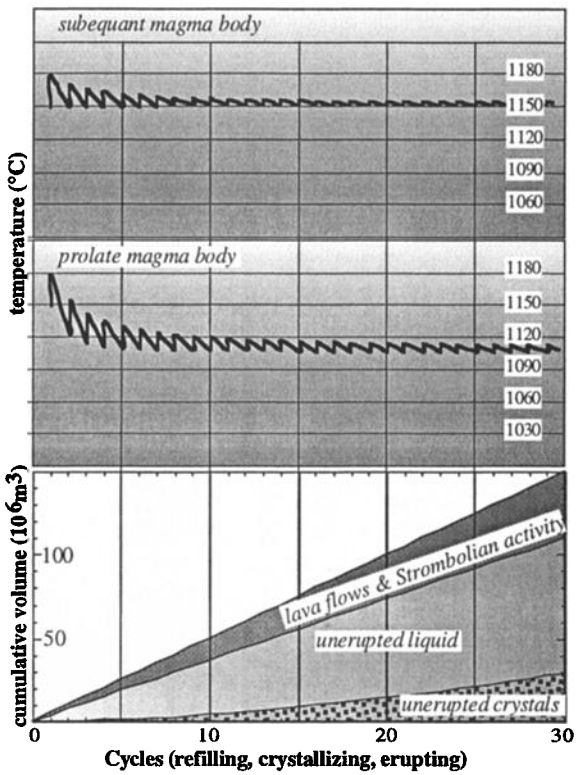

Figure 15. Semiquantitative analysis of the thermal evolution of a small, growing, periodically supplied, and tapped magma chamber. The shape constrains its final thermal state (upper and middle). The model was forced to fit the volume, composition, and phenocryst content of the 1906 eruption (data from *Santacroce et al.* [1993]). The thermal oscillations of the prolate body reproduce well the temperature evolution of the 1906 magma chamber as recorded by T_{hom} of MI from type 5 (Figure 1) pyroxenes. (bottom) The cumulative volume of erupted magma and of melt and crystals accumulating in the chamber during the 1872-1906 period, before being completely erupted in April 1906.

lates the temperature of the growing, convecting magma body, differently shaped (prolate or subequant), conductively cooling [*Marsh*, 1982] hosted in country rocks with a constant temperature (200°C). The shape and the volume of the body change according to its fixed vertical dimension (2000 m in the prolate case, 1000 m in the subequant case). Latent heats of crystallization and melting during mixing and fractionation were not taken into account. The oversimplifications of conductive cooling of the chamber and of constant temperature of the country rocks (aquifer-hosting lava pile or limestone [*Bernasconi et al.*, 1981; *Santacroce*, 1987]) are justified by the presence of a high-temperature thermometamorphic aureola lining the chamber. This aureola displaces the aquifer outward, leaving an internal conductive zone whose temperature increase is dampened by convection in the outer aquifers. Figure 15 shows that the process tends toward a thermal steady state where the temperature is mainly governed by the aspect ratio of the chamber (height/width). Prolate magma bodies rapidly lose heat due to their high surface/volume ratio, and steady state is characterized by a temperature significantly lower than the mafic influx. Thermal loss is less effective in subequant chambers.

Despite the limit of the gross simplifications used, the comparison of Figure 15 with the distribution of T_{hom} of MI in recurrently zoned type 5 pyroxenes (Figure 4) strongly suggests that these pyroxenes represent crystals formed at the walls of a prolate, dike-shaped chamber. They should have remained in the suspension zone [*Marsh*, 1989], recording and summarizing the thermal and compositional evolution of the resident magma, while crystallinity was low enough to allow convection and magma mixing. In the chamber, as a whole, temperature and degree of evolution of the magma decrease with time through oscillations of decreasing amplitude. The correspondence between the compositional ranges of erupted products (related to the different phenocryst contents of a thermally and compositionally homogeneous liquid) and MI (Figure 7) reflects the uniqueness of pyroxene as a mineral phase playing a role in the mixing-fractionation processes. The presence of MI having different T_{hom} and compositions in the different zones excludes the oscillatory zoning of Vesuvius pyroxenes as resulting from "intrinsic" mechanisms (feedback between crystal growth and solute diffusion or surface effects [*Shore and Fowler*, 1996]). On the contrary, it emphasizes the role of magma recharge as an "extrinsic" mechanism (variations in PT and melt composition), as a particular case of the mixing process already invoked to explain recurrently zoned pyroxene in Italian potassic magmas [*Barton et al.*, 1982].

The diopsidic cores of recurrently zoned 1906 pyroxenes contain MI whose maximum values of T_{hom} are slightly higher (~1200°C) than in the Pompeii and Avellino diopside (~1150°C) with an identical compositional range. This reflects the different extent of undercooling undergone by the mafic batches entering the different chambers. In fact, the mafic magma batches feeding the Avellino and Pompeii chambers mixed with larger, more evolved, cooler, resident bodies than those feeding the 1906-type chambers. Assuming a constant liquidus temperature of diopside ($^{di}T_{liq}$) for all Vesuvius magmas, this implies higher values of $^{di}T_{liq} - T_{hom}$ (approximately stronger undercooling) in the Avellino-Pompeii case. The occurrence of skeletal diopsidic cores in some type 3 and in type 5 pyroxenes also reveals rapidly formed undercooled crystals, probably related, in 1906, to the initial stages of the chamber.

5.2. Magma Chamber Evolution in Obstructed Conduit Conditions

Significant differences are observed in comparing the magma chambers emptied during the different eruptions.

5.2.1. Plinian chambers: Avellino and Pompeiii. The detailed study of the A.D. 79 "Pompeii" deposits allowed *Cioni et al.* [1995] to present a model of the Pompeii magma chamber characterized by a subequant shape and a main twofold layering, with a phonolitic "white magma" (T°C=850-900) separated from a phonotephritic "grey" magma (T°C=1000-1100) by a diffusive interface. The Avellino deposits resemble those of Pompeii in that they are characterized by a discontinuous variation from early erupted phonolitic white pumice to late erupted tephriphonolitic grey pumice. Mineralogical [*Marianelli*, 1995] and MI data (Table 6 and Figure 8) show that (1) white pumice resulted from the emission of alkali-phonolitic to phonolitic melts ranging in temperature from 800-850°C (phenocrysts of cpx $_{Fs25-30}$ and $Kfp_{Or65-70}$) to 900-950°C (cpx $_{Fs20}$ and Kfp_{Or80}); (2) grey pumice testifies to the emission of hybrid tephriphonolitic magma formed during extensive syneruptive mixing between the "white" melts (same cpx-Kfp pairs than in white pumice) and a phonotephritic melt (phenocrysts of cpx $_{Fs10-15}$, no Kfp) with temperature of 1040-1070°C.

Together with whole rock compositional variations (Figure 12), these data can be interpreted in terms of an Avellino magma chamber quite similar to that of Pompeii. Both chambers were characterized by a main twofold layering strongly contrasting in temperature and composition, the main difference concerning the overheated state of the tephriphonolitic Pompeii lower body (no liquidus phases were found [*Cioni et al.*, 1995]). The dynamics of extraction was also similar, with extensive mixing occurring throughout the second half of the eruption (emission of hybrid tephriphonolitic grey pumice rapidly formed within the chamber as a consequence of syneruptive mixing) and no emission of not mixed lower magma.

5.2.2. Sub-Plinian chambers: Pollena. The A.D. 472 "Pollena" deposits exhibit an almost continuous compositional variation from initially erupted leucititic phonolite to later erupted leucititic phonotephrite [*Rosi and Santacroce*, 1983; *Marianelli*, 1995]. The phenocryst assemblages of pumice samples collected at different heights in the deposit show a variability that suggests equilibrium with the matrix glass and coherence with temperature variation and MI composition (Figure 16 and Table 7). Syneruptive mixing phenomena were therefore moderate and never involved liquids with strongly contrasting temperature and composition. All these observations suggest that the Pollena eruption tapped a medium aspect ratio (cigar-like) magma chamber with an almost continuous thermal/compositional gradient.

5.2.3. "Rejuvenated" chambers: AP1 and AP4. The AP1 and AP4 eruptions have sizes similar or smaller than the Pollena eruption. *Andronico et al.* [1995] suggested that they repeatedly tapped the upper portions of a rejuvenated magma chamber in which a substantial residual of the Avellino tephriphonolitic, hybrid "grey" magma continued to be supplied and evolve. The final stage of this process is represented by the Pompeii eruption, whose "Avellino heritage" has been invoked by *Civetta et al.* [1991] and *Cioni et al.* [1995]. The bimodal T_{hom} distribution shown by MI in both AP1 and AP4 (Figure 8) could reflect the repeated attempt of the resident magma to evolve toward a Plinian, twofold

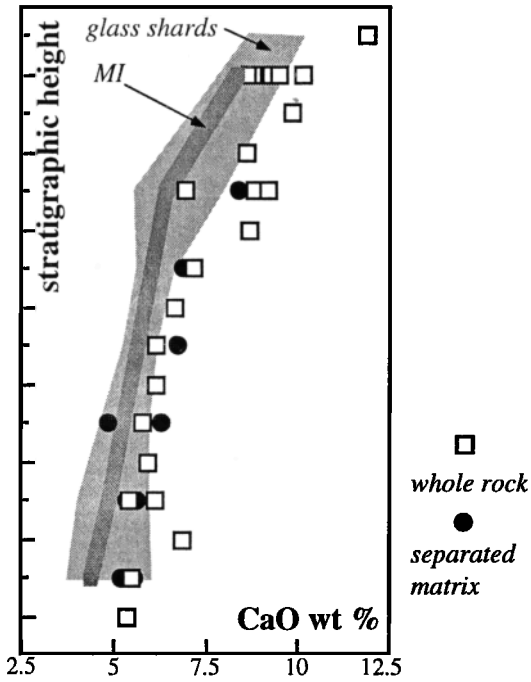

Figure 16. Variations of CaO content with stratigraphic height in the Pollena deposits. The absence of syneruptive mixing between strongly contrasting liquids is revealed by the covariations of glass (both as matrix shards and MI in pyroxene) and whole rock.

chamber by developing highly evolved "white" phonolitic caps. The poorly variable tephriphonolitic composition of AP pumice sharply contrasts with the highly heterogeneous pyroxene, MI and T_{hom}. This fact and the glassy (quenched) nature of all MI in AP salitic pyroxenes suggest an almost instantaneous, syneruptive mixing involving the simultaneous extraction of magma from both an upper, layered, thin "white" body and a lower, probably convective, large "grey" body.

6. Summary and Conclusions

Clinopyroxene phenocrysts with their MI give insights as to the different evolution of the plumbing system of Vesuvius during periods of open or obstructed conduit conditions. In both cases the system is constantly characterized by the presence of shallow reservoirs whose deep magma supply occurs through discrete mafic batches, whose compositional spectrum is reflected by the MI in diopsidic pyroxene. The data presented confirm a change from K-basaltic to K-tephritic deep magmas [*Marianelli et al.*, 1995], indicating this change occurred after AP1 (around 3000 years B.P.) and before the A.D. 79 eruption.

When the conduit is open (e.g., 1906), a small reservoir (10^7-10^8 m^3) progressively forms. The MI summarize the evolution of resident magma throughout the (short) life time of the chamber, characterized by an easy thermal perturbability of the resident magma due to its moderate volume. The oscil-

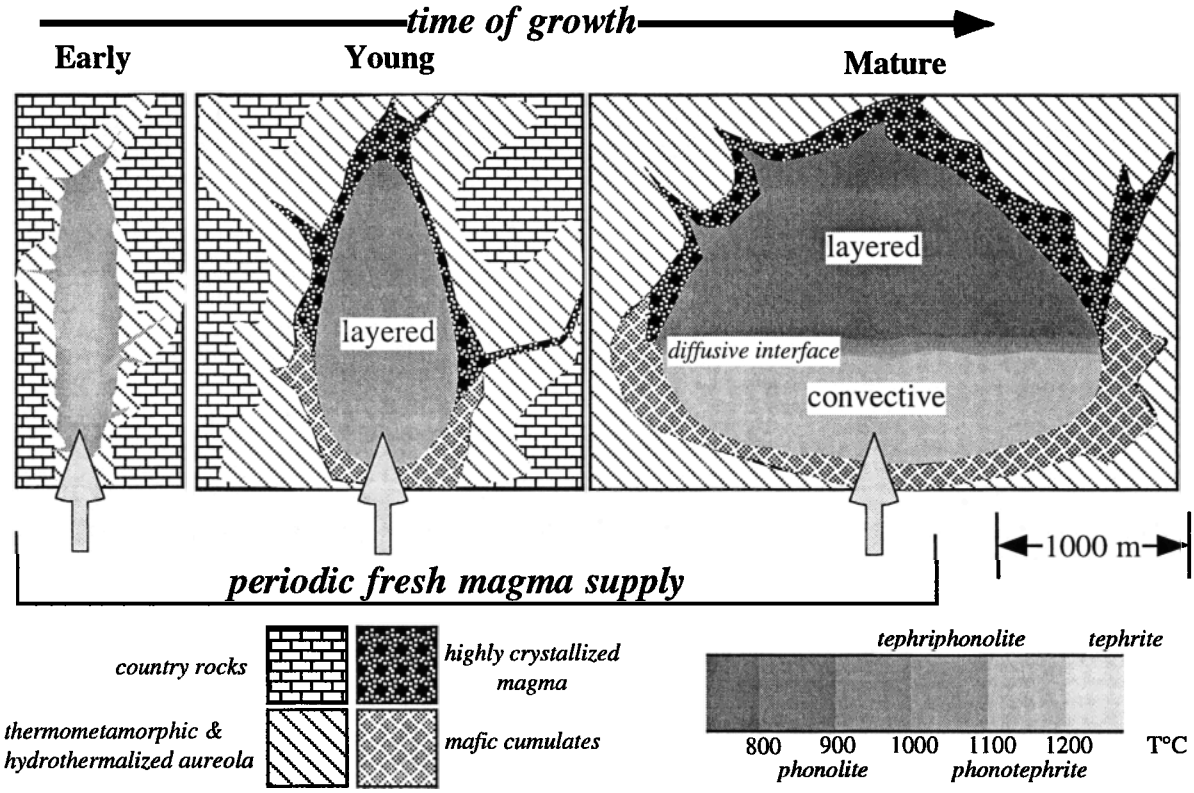

Figure 17. Highly speculative sketch of the suggested evolutionary stages of Vesuvius magma chambers. The chambers grow following the periodic tephritic inputs and expand mainly laterally, decreasing their aspect ratio (height/width) while changing their compositional layering. Scale was assumed on the basis of studied cases [*Santacroce et al.*, 1993; *Marianelli*, 1995; *Cioni et al.*, 1995]. Temperature and composition are from MI in pyroxene.

latory zoning of pyroxene and the variability of T_{hom} of MI within single crystals record these thermal and compositional fluctuations, with "hot" diopsidic zones marking the recurrent hot magma inputs.

When the conduit is obstructed, magma chambers form and grow through periodic arrival of deep magma batches. We suggest that the increasing volume is accompanied by changes in the aspect ratio of the chamber as well as in the main compositional layering (Figure 17): (1) initial stage, high aspect ratio chamber similar to the "1906," open conduit conditions, chamber, moderate volume (0.01-0.1 km^3), almost homogeneous mafic melt downward enriched in crystals [*Santacroce et al.,* 1993]; (2) young stage, medium aspect ratio "Pollena-type" chamber, medium volume (0.1-0.5 km^3), gradual, almost continuous gradient from mildly evolved to felsic melt [*Marianelli,* 1995]; (3) mature stage, low aspect ratio "Pompeii-type" chamber, large volume (0.5-5 km^3), twofold layering with stepwise gradient separating the lower, convective, mildly evolved portion from the upper, statically stratified, felsic portion [*Cioni et al.,* 1995].

The age (and size) of the magma chamber alone does not seem sufficient to determine the magnitude of an eruption. AP eruptions repeatedly tapped a mature chamber without reaching Plinian magnitudes. Differently from the Plinian chambers, in the AP cases the upper, evolved, "white" caps did not have time to reach a volume large enough to be tapped without being mixed with the lower "grey" tephriphonolitic layer during the eruption. The thickness of white magma in the chamber should have been in fact lower than the minimal magma withdrawal depth [*Blake and Yvey,* 1986; *Spera et al.,* 1986; *Sigurdsson et al.,* 1990]. In the AP cases, much of the "grey" magma remained unerupted. We can speculate that a large, "white," volatile-rich upper cap is a necessary condition for involving in the eruption most of the lower, hot, convective, "grey" magma [*de Silva and Wolff,* 1995].

The cases studied seem to suggest slightly variable temperatures (1050°-1100°C) for this lower "grey" body (which has rather different compositions: phonotephritic in Avellino, and tephriphonolitic, overheated, in Pompeii) as well as for the basal portion of the upper white stratified magma (900°-950°C). These values could suggest invariant thermal conditions for the diffusive interface separating the two bodies. The evolutionary stage of the chamber would then be reflected by the position of the boundary layer (i.e., by the mass ratio between grey hot (T~1050°C) and white cool (T<900°C) melts). This implies that the "old" Vesuvius chamber could be composed almost entirely of felsic evolved melts, with a quite reduced, or absent, convective grey portion.

Finally, the presented data allowed definition of the composition-temperature field of Vesuvius magmas emphasizing the role of magma refilling in extending the compositional range to the generation of highly alkaline melts, probably inconsistent with a closed system evolution. This conclusion could have general validity for the entire Italian potassic province. When considering their petrogenesis, we propose that the mere presence of K-phonolitic melts should suggest a periodically refilled shallow magma chamber.

Acknowledgments. This paper benefitted from the review of Marc Defant, René Maury, and an anonymous referee. Their constructive comments and suggestions greatly improved the quality of the manuscript. The research was sponsored by CNR (National Council of Research of Italy), Gruppo Nazionale per la Vulcanologia.

References

Andronico, D., R. Cioni, P. Marianelli, and A. Sbrana, InterPlinian activity at Somma-Vesuvius: the Avellino-Pompeii period, *Period. Mineral., 64,* 79-80, 1995.

Arnò, V., C. Principe, M Rosi, R. Santacroce, A. Sbrana, and M.F. Sheridan, Eruptive history, in *Somma-Vesuvius,* edited by R. Santacroce, *CNR Quad. Ric. Sci. 114*(8), 53-103, 1987.

Barberi, F., H Bizouard, R. Clocchiatti, N. Metrich, R. Santacroce, and A. Sbrana, The Somma-Vesuvius magma chamber: A petrological and volcanological approach, *Bull. Volcanol., 44,* 295-315, 1981.

Barberi, F, R. Cioni, R. Santacroce, A. Sbrana, and R. Vecci, Magmatic and phreatomagmatic phases in explosive eruptions of Vesuvius as deduced by grain-size and component analysis of the pyroclastic deposits, *J. Volcanol. Geotherm. Res., 38,* 287-307, 1989.

Barton, M., J.C. Varekamp, and M.J. Van Bergen, Complex zoning of clinopyroxenes in the lavas of Vulsini, Latium, Italy: Evidence for magma mixing, *J. Volcanol. Geotherm. Res., 14,* 361-388, 1982.

Belkin, H.E., R.J. Kilburn, and B. De Vivo, Sampling and major element chemistry of the recent (A.D. 1631-1944) Vesuvius activity, *J. Volcanol. Geotherm. Res., 58,* 273-290, 1993.

Belkin, H.E., B. De Vivo, K. Torok, and J.D. Webster, Silicate-melt inclusions in Vesuvius lavas (<1631 A.D.): Microthermometry and analytical chemistry, paper presented at Pan-American Current Research on Fluid Inclusions, PACROFI, Madison, Wisc., May 30 to June 1, 1996.

Bernasconi, A., P. Bruni, L. Gorla, C. Principe, and A. Sbrana, Risultati preliminari dell'esplorazione geotermica profonda nell'area vulcanica del Somma-Vesuvio, *Rend. Soc. Geol. It., 4,* 237-240, 1981.

Bertagnini A., P. Landi, R. Santacroce, and A. Sbrana, The 1906 eruption of Vesuvius: From magmatic to phreatomagmatic activity through the flashing of a shallow depth hydrotermal system, *Bull. Volcanol., 53,* 517-532, 1991.

Blake, S., and G.N. Ivey, Magma-mixing and the dynamics of withdrawal from stratified reservoirs, *J. Volcanol. Geotherm. Res., 27,* 153-178, 1986.

Carey, S., and H. Sigurdsson, Temporal variations in column height and magma discharge rate during the 79 A.D. eruption of Vesuvius, *Geol. Soc. Am. Bull., 99,* 303-314, 1987.

Carta, S., R. Figari, G. Sartoris, E. Sassi, and R. Scandone, A statistical model from Vesuvius and its volcanological implications, *Bull. Volcanol., 44,* 2, 129-151, 1981.

Cioni, R., P Marianelli, and A. Sbrana, L'eruzione del 79 d.C.: Stratigrafia dei depositi ed impatto sugli insediamenti romani nel settore orientale e meridionale del Somma-Vesuvio, *Riv. Studi Pompeiiani, IV,* 179-198, 1990.

Cioni, R., P. Marianelli, and A. Sbrana, Dynamics of the A.D. 79 eruption: Stratigraphic, sedimentological and geochemical data on the successions from the Somma-Vesuvius southern and eastern sectors, *Acta Vulcanol., Marinelli Vol., 2,*109-123, 1992.

Cioni, R., L. Civetta, P. Marianelli, N. Metrich, R. Santacroce, and A. Sbrana, Compositional layering and syneruptive mixing of a periodically refilled shallow magma chamber: The AD 79 Plinian eruption of Vesuvius, *J. Petrol., 36,* 3, 739-776, 1995.

Civetta, L., and R. Santacroce, Steady-state magma supply in the last 3400 years of Vesuvius activity, *Acta Vulcanol., Marinelli Vol.,* 2, 147-159, 1992.

Civetta, L., R. Galati, and R. Santacroce, Magma mixing and convective compositional layering within the Vesuvius magma chamber, *Bull. Volcanol., 53,* 287-300, 1991.

de Silva, S.L., and J.A. Wolff, Zoned magma chambers: The influence of magma chamber geometry on sidewall convective fractionation, *J. Volcanol. Geotherm. Res., 65,* 111-118, 1995.

Ghiorso, M.S., and R.O. Sack, Chemical mass transfer in magmatic processes, IV, A revised and internally consistent thermodynamic model for the interpolation and extrapolation of liquid-solid equilibria in magmatic systems at elevated temperatures and pressures, *Contrib. Mineral. Petrol., 119,* 197-212, 1995.

Lacroix, A., Les laves leucitiques de la Somma, *C. R. Hebd. Acad. Sci. Paris, 165,* 481-487, 1917.

Le Bas, M.J., R.W. Le Maitre, A. Streckeisen, and B. Zanettin, A chemical classification of volcanic rocks based on the total alkali-silica diagram, *J.Petrol., 27,* 745-750, 1986.

Lirer, L., T. Pescatore, B. Booth, and G.P.L. Walker, Two Plinian pumice-fall deposits from Somma-Vesuvius, Italy, *Geol. Soc. Am. Bull., 84,* 759-772, 1973.

Lirer, L., R. Munno, P. Petrosino, and A. Vinci, Tephrostratigraphy of the A.D. 79 pyroclastic deposits in the perivolcanic area of Vesuvius (Italy), *J. Volcanol. Geotherm. Res., 58,* 133-149, 1993.

Marianelli, P., La camera magmatica del Vesuvio: Processi petrogenetici e dinamica eruttiva, Ph.D. thesis, Univ. degli Studi di Pisa, Pisa, Italy, 1995.

Marianelli, P., N. Metrich, R Santacroce, and A. Sbrana, Mafic magma batches at Vesuvius· A glass inclusion approach to the modalities of feeding stratovolcanoes, *Contrib Mineral. Petrol., 120,* 159-169, 1995.

Marsh, B.D., On the mechanics of igneous diapirism, stoping, and zone melting, *Am. J. Sci., 282,* 808-855, 1982.

Marsh, B.D., Magma chambers, *Annu. Rev. Earth Planet. Sci., 17,* 439-474, 1989.

O'Hara, M J., Geochemical evolution during fractional crystallization of a periodically refilled magma chamber, *Nature, 266,* 503-507, 1977.

Quareni, F, and F. Mulargia, Modeling the closure of volcanic conduits with an application to Mount Vesuvius, *J. Geophys Res.,* 98, 4221-4229, 1993.

Rahman, S., Some aluminous clinopyroxenes from Vesuvius and Mt. Somma, Italy, *Mineral. Mag., 40,* 43-53, 1975.

Roedder, E., Fluid inclusions, *Rev. Mineral.,* vol. 12, 646 pp., Mineral. Soc. of Am., Washington, D.C., 1984.

Rolandi, G., G. Mastrolorenzo, A.M. Barrella, and A. Borrelli, The Avellino Plinian eruption of Somma-Vesuvius (3,760 y.B.P.): The progressive evolution from magmatic to hydromagmatic style, *J. Volcanol. Geotherm. Res., 58,* 67-88, 1993

Rosi, M, and R. Santacroce, The A.D. 472 "Pollena" eruption: Volcanological and petrological data for this poorly-known, Plinian-type event at Vesuvius, *J Volcanol. Geotherm. Res., 17,* 249-271, 1983.

Santacroce, R., A general model for the behavior of the Somma-Vesuvius volcanic complex, *J. Volcanol. Geotherm. Res., 17,* 237-248, 1983.

Santacroce, R. (Ed.), *Somma-Vesuvius, CNR Quad. Ric. Sci., 114* (8), 230 pp., 1987.

Santacroce, R., A. Bertagnini, L Civetta, P. Landi, and A. Sbrana, Eruptive dynamics and petrogenetic processes in a very shallow magma reservoir: The 1906 eruption of Vesuvius, *J. Petrol., 34,* 383-425, 1993.

Santacroce, R , R. Cioni, L. Civetta, P. Marianelli, N. Metrich, and A. Sbrana, How Vesuvius works, *Atti Conv. Lincei, 112,* 185-196, 1994.

Santacroce, R., R Cioni, P. Marianelli, and A Sbrana, Understanding Vesuvius and preparing for its next eruption, in *The Cultural Response to the Volcanic Landscape,* edited by M.S. Balmuth, Tufts Univ., Medford, Mass., in press, 1998.

Sheridan, M.F., F. Barberi, M. Rosi, and R. Santacroce, A model for Plinian eruptions of Vesuvius, *Nature, 289,* 282-285, 1981.

Shore, M., and A.D. Fowler, Oscillatory zoning in minerals: A common phenomenon, *Can. Mineral., 34,* 1111-1126, 1996.

Sigurdsson, H., S. Cashdollar, and R.S.J. Sparks, The eruption of Vesuvius in A.D. 79: Reconstruction from historical and volcanological evidence, *Am. J. Archeol., 86,* 39-51, 1982.

Sigurdsson, H., S. Carey, W. Cornell, and T. Pescatore, The eruption of Vesuvius in A.D 79, *Nat. Geogr. Res., 1,* 332-387, 1985.

Sigurdsson, H., W. Cornell, and S. Carey, Dynamics of magma withdrawal during the 79 A.D. eruption of Vesuvius, *Eos Trans. AGU, 68*(16), 434, 1987.

Sigurdsson, H., W. Cornell, and S. Carey, Influence of magma withdrawal on compositional gradients during the AD 79 Vesuvius eruption, *Nature, 345,* 519-521, 1990.

Sobolev, A V., L.V. Dmitriev, V.L. Barsukov, V.N. Nevsorov, and A.V. Slutsky, The formation conditions of high magnesium olivines from the monomineral fraction of Luna-24 regolith, *Lunar Planet. Sci Conf., 11th,* 105-116, 1980.

Sobolev, A , M.V. Portnyagin, L.V. Dmitriev, O.P. Tsmeryan, L.V. Danyushevsky, N.N. Kononkova, N. Shimizu, and P.T. Robinson, Petrology of ultramafic lavas and associated rocks of the Troodos Massif, Cyprus, *Petrology, 4,* 331-361, 1993.

Spera, F.J., D.A. Yuen, J.C. Greer, and G. Sewell, Dynamics of magma withdrawal from stratified magma chambers, *Geology, 14,* 723-726, 1986

Tait, S, Selective preservation of melt inclusions in igneous phenocrysts, *Am. Mineral., 77,* 146-155, 1992.

Thompson, R.N., Oscillatory and sector zoning in augite from Vesuvian lava, *Year Book, Carnegie Inst. Washington, 71,* 463-470, 1972.

Vaggelli, G., H.E. Belkin, B. De Vivo, and R Trigila, Silicate-melt inclusions in recent Vesuvius lavas (A.D. 1631-1944), I, Petrography and microthermometry, *Eur. J. Mineral., 4,* 1113-1124, 1992.

Vaggelli, G., B. De Vivo, and R. Trigila, Silicate-melt inclusions in recent Vesuvius lavas (1631-1944), II, Analytical chemistry, *J. Volcanol. Geotherm. Res., 58,* 367-376, 1993.

Villemant, B., R. Trigila, and B. De Vivo, Geochemistry of Vesuvius volcanics during 1631-1944 period, *J. Volcanol. Geotherm. Res., 58,* 291-313, 1993.

Washington, H S., and H.E Merwin, Note on augite from Vesuvius and Etna, *Am. J. Sci., 1,* 20-30, 1921.

Zambonini, F., Mineralogia Vesuviana, *Atti R. Accad. Sci. Fis Mat. Nat , Napoli 2a, 14, 7,* 1910

R. Cioni, P. Marianelli, and R. Santacroce, Dipartimento di Scienze della Terra, Università degli Studi di Pisa, via Santa Maria, 53, 56126 Pisa, Italy (e-mail: cioni@dst.unipi.it; marianelli@dst.unipi.it; santacroce@dst.unipi.it)

(Received August 6, 1997; revised February 11, 1998; accepted March 31, 1998.)